

Multiple-scattering theory of X-ray absorption: a review

This article has been downloaded from IOPscience. Please scroll down to see the full text article.

1992 J. Phys.: Condens. Matter 4 8269

(<http://iopscience.iop.org/0953-8984/4/43/004>)

View [the table of contents for this issue](#), or go to the [journal homepage](#) for more

Download details:

IP Address: 171.66.16.96

The article was downloaded on 11/05/2010 at 00:43

Please note that [terms and conditions apply](#).

REVIEW ARTICLE

Multiple-scattering theory of x-ray absorption: a review

Luciano Fonda

Sincrotrone Trieste, Padriciano 99, Trieste, Italy, and International Centre for Theoretical Physics, Trieste, Italy

Received 30 December 1991, in final form 16 July 1992

Abstract. We review the basic elements of the theory of x-ray absorption using the tools provided by the theory of multiple scattering. We first use an approximate momentum space approach which gives a very clear physical insight where the final formulas expressing EXAFS and XANES, i.e. the structures appearing in the absorption coefficient above the edge of a deep core-level threshold, are given in terms of eigenstates of the photoelectron momentum. We then review the correct formalism, the curved-wave theory, for which we need to work in angular momentum space. Simple graphic representations are given for the multiple-scattering function.

Contents

1. Introduction
2. Multiple-scattering theory of the photoemission process
3. The photoemission cross section and the multiple-scattering function $\chi_{L,L'}$
4. The momentum space approach
5. The curved-wave theory
 - 5.1. The formalism in angular momentum space
 - 5.2. Inelasticities and disorder
 - 5.3. The full solution

1. Introduction

The history of the explanation of the oscillatory structure appearing in the x-ray absorption coefficient of a complex molecular or condensed system, as a function of the x-ray energy above the edge of a core-level threshold, called *extended x-ray absorption fine structure* (EXAFS), is long and varied.

It was first recognized by Kronig and Petersen [1-3] that the explanation of the phenomenon lies in the existence of final-state interactions (see [4, 5] for a history of the subject). The final state of the photoelectron is modified, as compared to the photoemission from an isolated atom, by the presence of an environment. The systematic quantum mechanical treatment, initiated by the seminal papers of Lytle, Sayers and Stern [6, 7], anticipated that the EXAFS technique can actually yield structure information on the material, particularly in situations where other techniques, such as diffraction, are not available. The photoelectron, in the

process of repeated scatterings from the atoms of the condensed system before going out of the material, collects information on the system itself particularly on the neighbours of the atom absorber. These papers produced a proliferation of contributions [8–42] (for reviews see references [43–50]) who refined the physical interpretation of the process—including the possibility of understanding also the *x-ray absorption near-edge structure* (XANES) using the tools provided by the multiple-scattering approach [51–63]—and pointed out its wide applicability. By comparing theory with the experimental data, detailed information can be obtained on the local atomic environment, out to few (about 3.5–5) Å, around the photoabsorber. For compounds, it is possible to investigate the local order around each type of atom separately, by analysing the EXAFS spectra on each absorption edge. This atomic information is extracted without the need of an electronic structure calculation and, most important of all, for ordered as well as disordered systems. The sample may be a gas, liquid, solid (crystalline or amorphous), diluted in a solution, a living cell etc.

Lately, there has been a great revival and enhancement of such a tool of scientific research, with the possibility of using intense brilliant sources such as synchrotron radiation accelerators. Applications now encompass almost all fields, in particular catalysis, chemistry, geology, life sciences, materials science, surface physics etc.

In this article, we review the basic elements of the theory of x-ray absorption fine structure by using the tools provided by the theory of multiple scattering†. In section 2 we prove in general the multiple-scattering formulas, relevant for our case, by employing the Green's operator approach in the Hilbert space of the scattering states of the system. Section 3 contains technical details, useful for the evaluation of the multiple-scattering function. In section 4 we introduce an approximate momentum space formalism, in which the final formulas are expressed in terms of eigenstates of the photoelectron momentum. The perturbative expansion obtained gives a very clear physical insight into the rather complicated process of photoabsorption. In section 5 we then treat the correct approach, which we call *curved-wave theory* for which use is made of the angular momentum representation. Simple graphic representations of the multiple-scattering function are given for both formulations. In section 5 we also discuss briefly the full solution which one is able to obtain using computer programs [65–71] in order to describe XANES when the perturbation expansion fails to converge.

2. Multiple-scattering theory of the photoemission process

We shall consider the x-ray absorption from a material, a complex molecular or condensed system (liquid, amorphous or crystalline), and shall tune the x-rays at energies above the threshold for the excitation of a deep core level of a specific chemical element. Experimentally one determines μ_c , the contribution to the x-ray absorption coefficient due to the excitation of the core level c . The coefficient μ_c is given by:

$$\mu_c = n_c \sigma_c \quad (2.1)$$

† For completeness of information, it must be said that for crystalline systems the traditional approach is that based on band-structure methods (see for example [64] and references therein). The applicability of these calculations is, however, limited to systems with perfect crystalline order, since any minor deviation from translational symmetry requires an extension of band theory. Hence the atomic structure is here an input rather than an inference. For a comparison between band structure and multiple-scattering approaches see [8, 25, 33].

where n_c is the density of atoms with the core level c of concern and σ_c the absorption atomic cross section from this level.

As a function of the energy $\hbar\omega$ of the incoming photon, in the region just before the threshold, σ_c presents a resonant structure which contains information about the binding energies, quantum numbers and multiplicities of low-lying energy levels. At the threshold, σ_c exhibits a finite jump, called the *absorption edge* (its analytic expression for hydrogen-like atoms is given, for example, in [72]), as a result of the Coulomb attraction experienced by the ejected photoelectron. The edge shows up also in elastic and inelastic cross sections already existing at that energy (see [73] and references therein).

Above the absorption edge, σ_c shows a marked fine structure, called XANES when near (usually up to 50 eV above the edge), and EXAFS when away from the edge and extending well beyond, usually up to 1000 eV above (some authors use the acronym XAFS to cover all the range). In contrast, for isolated atoms the absorption cross section does not show any marked oscillatory behaviour, decreasing smoothly as a function of the energy beyond the edge. XANES and EXAFS are then caused by the presence of the environment around the absorbing atom in the condensed material.

The absorption cross section σ_c , apart from a background—in general slowly varying in energy in the region of interest, due to inelastic scatterings—can be identified with the photoemission cross section integrated over angles and summed over final spin and over the initial degeneracies of the completely filled core-level c (which we shall call the total photoemission cross section).

In order to evaluate σ_c , we shall consider the photoemission T -matrix†, to be evaluated on the energy shell, to the first order in the incoming photon field:

$$T_{f-i} = \langle \Psi_f^{(Z)} | \langle 0 | \left(-\frac{e}{mc} \sum_{j=1}^Z \mathbf{A}(\mathbf{r}_j) \cdot \mathbf{p}_j \right) | 1_i \rangle | \Psi_i^{(Z)} \rangle \quad (2.2)$$

where \mathbf{p}_j is the momentum operator of the j th electron and m its mass; $\mathbf{A}(\mathbf{r}_j)$ is the quantized radiation field (in the Coulomb gauge $\nabla_j \cdot \mathbf{A}(\mathbf{r}_j) = 0$) evaluated at the position of the j th electron.

The initial state vector is the product of the incoming photon state vector $|1_i\rangle$ times the initial Z -electron atomic normalized bound state vector $|\Psi_i^{(Z)}\rangle$. The final state is given by the product of the photon vacuum $|0\rangle$ times the state $|\Psi_f^{(Z)}\rangle$ describing an emitted electron and the ionized $(Z-1)$ -electron atom in which a deep core hole witnesses the absorption of the initial photon. Due to the decrease in screening of the nuclear attraction, the electrons left in the ionized atom draw a little closer to the nucleus.

A major simplification of the many-body amplitude (2.2) is obtained from the fact that it is possible to explain the main features of x-ray absorption through the change of state of a single electron [74, 75, 18]. Use of the sudden approximation, within the framework of a Hartree-Fock-Slater treatment of the states describing the initial and the final atoms, enables the factorization of those states reducing (2.2) to the single-particle amplitude

$$T_{f-i} = F_0 \langle \psi_f^{(-)} | \langle 0 | H_I | 1_i \rangle | \psi_c \rangle. \quad (2.3)$$

† For the definition of the T -matrix and cross sections, I follow [73].

The interaction is now effective only on the *active* emitted electron:

$$H_I = -(e/mc)A \cdot p \quad (2.4)$$

$|\psi_c\rangle$ and $|\psi_f^{(-)}\rangle$ are now single-particle states. The vector $|\psi_c\rangle$ represents the initial single-electron normalized bound state relative to the core level c . $|\psi_f^{(-)}\rangle$ is the final single-electron scattering state as resulted from the interaction of the emitted photoelectron with:

- (i) the completely relaxed (i.e. lowest-energy configuration of the *passive* $Z - 1$ electrons in the presence of the core hole) ionized absorbing atom A ;
- (ii) the neighbours of A in the condensed material.

$F_0 \equiv \langle \psi_f^{(Z-1)} | \psi_i^{(Z-1)} \rangle$ is the $Z - 1$ -passive-electrons overlap integral. Its modulus is less than 1; therefore it correspondingly decreases the amplitude of the cross section. $|F_0|^2$ has normally values between 0.6 and 0.9 [21, 76].

The single-particle approach (2.3) works nicely at energies away from the threshold, in the EXAFS region, where the active electron scarcely intermingles with the other electrons of the system.

Close to threshold, in the XANES region, x-ray absorption from deep core levels is still dominated by single-electron transitions (at variance with soft x-ray absorption at the edges of shallow core-level excitations which is dominated by many-body effects); however, many-body effects appear. For example, up to about 10–20 eV, where the interaction of the photoelectron with the passive electrons becomes strong, the probability for the excitation or ionization (shake-up-shake-off) of other electrons becomes sizeable. In experiments performed in this energy range, small threshold anomalies corresponding to these processes show up in the cross section (see, for example, [77, 78]); the photoelectron cannot be considered as a ‘spectator’ of the relaxation process and may cause anisotropies in this process [79]; typical autoionizing many-body excited states may occur and produce resonant effects on the cross section [80, 81].

The effects of these (low-energy) phenomena are correctly included in the many-body amplitude (2.2). Therefore, in applying the single-particle scheme (2.3) to x-ray absorptions from deep core levels, we have to keep in mind that at energies close to the edge, equation (2.3) will yield some departures from the experimental data.

For simplicity we shall deal only with spin-independent interactions so that our photoelectron can be considered as *spinless*. The generalization to include the photoelectron spin is, however, straightforward [28, 42, 61, 62]. Furthermore, we shall consider only elastic scattering from the relaxed ionized atom A and from its neighbours. The inclusion of inelasticities, of many-body effects such as electron-electron scattering, of the Auger and radiative decay of the core hole and of thermal vibrations is not trivial. Most commonly, one introduces proper damping factors in the final formulas to simulate their effect (the discussion on these points is postponed to section 5).

In (2.3), the vector $|\psi_f^{(-)}\rangle$ is a ‘mathematical’ state, an eigenstate of the total final state (Hermitian) effective single-particle electron’s Hamiltonian H_f , which satisfies incoming wave boundary conditions. It is connected to the ‘physical’ state $|\psi_f^{(+)}\rangle$, which obeys outgoing wave boundary conditions, through time reversal invariance (see, for example, [82], chapter 2.7):

$$\psi^{(-)}(\mathbf{k}_f, \mathbf{r}) = [\psi^{(+)}(-\mathbf{k}_f, \mathbf{r})]^* \quad (2.5)$$

where $\hbar k_f$ is the momentum of the photoelectron. The states $|\psi^{(\pm)}(\mathbf{k})\rangle$ are normalized exactly to a three-dimensional Dirac δ -function:

$$\langle \psi^{(\pm)}(\mathbf{k}) | \psi^{(\pm)}(\mathbf{k}') \rangle = \delta^3(\mathbf{k} - \mathbf{k}').$$

The total photoemission cross section is given by

$$\sigma_c = 2 \sum_{m_i} \left(\frac{2\pi}{\hbar} \right)^4 \frac{m \hbar k_f}{c} \int d\Omega_f |T_{f-i}|^2 \quad (2.6)$$

where m_i labels the orbital angular momentum degeneracy of the core level c and the factor 2 represents the two electrons lying on the level (E_c, l_i, m_i) .

Writing the final energy as $E_f = \hbar^2 k_f^2 / 2m + \text{constant}$, we can write

$$d^3 k_f = (m/\hbar^2) k_f dE_f d\Omega_f.$$

For the total photoemission cross section σ_c we therefore get

$$\sigma_c = F_1 \sum_{m_i} \int d^3 k_f \delta(E - E_f) |\langle \psi_f^{(-)} | (H_I)_{01} | \psi_c \rangle|^2 \quad (2.7)$$

where $E = \hbar\omega + E_c$ is the total initial energy, $F_1 = [2(2\pi)^4/\hbar c] |F_0|^2$ and $(H_I)_{01} = \langle 0 | H_I | 1_i \rangle$.

Since $|\psi_f^{(-)}\rangle$ is eigenstate of the Hamiltonian H_f , belonging to the eigenvalue E_f , we can write

$$\sigma_c = F_1 \sum_{m_i} \langle \psi_c | (H_I)_{10} \delta(E - H_f) \left(\int d^3 k_f |\psi_f^{(-)}\rangle \langle \psi_f^{(-)}| \right) (H_I)_{01} | \psi_c \rangle.$$

The quantity in round brackets appearing at the RHS is almost a resolution of the identity

$$\int d^3 k_f |\psi_f^{(-)}\rangle \langle \psi_f^{(-)}| = I - \sum_{\text{bound states}} |\psi_b\rangle \langle \psi_b|$$

However, application of the operator $\delta(E - H_f)$ eliminates the contribution of the bound states:

$$\delta(E - H_f) |\psi_b\rangle = \delta(E - E_b) |\psi_b\rangle = 0$$

since $E > E_b$. For σ_c we then finally get

$$\sigma_c = F_1 \sum_{m_i} \langle \psi_c | (H_I)_{10} \delta(E - H_f) (H_I)_{01} | \psi_c \rangle. \quad (2.8)$$

In order to evaluate (2.8), we write $\delta(E - H_f)$ in terms of the complete Green's function G defined by

$$G = 1/(E + i\epsilon - H_f) \equiv P/(E - H_f) - i\pi\delta(E - H_f) \quad (2.9)$$

where the limit $\epsilon \rightarrow 0^+$ is understood and P means 'principal value'. Introducing G^\dagger , the Hermitian conjugate of the propagator G , we get

$$\delta(E - H_f) = (i/2\pi)(G - G^\dagger). \quad (2.10)$$

We finally obtain (here Im means 'imaginary part of')

$$\sigma_c = -\frac{F_1}{\pi} \sum_{m_i} \text{Im} \langle \psi_c | (H_I)_{i0} G (H_I)_{0i} | \psi_c \rangle. \quad (2.11)$$

As the photoelectron is emitted, it first feels the potential U_a of the ionized atom A in its fully relaxed state. It is then convenient to separate this contribution from the complete Green's function G .

The Hamiltonian H_f can be written as

$$H_f = K + U_a + \sum_{n \neq a} U_n \quad (2.12)$$

where K is the photoelectron kinetic energy and $\sum_{n \neq a} U_n$ is the sum of all the potentials exerted on the photoelectron by the neighbouring atoms. We deal with atoms embedded in an interstitial space of constant potential. This (muffin-tin zero) level determines our zero of energy. The atoms are supposed to be fully screened so that the photoelectron feels finite-range spherically symmetric non-overlapping local potentials U_n . This is the so-called *muffin-tin potential model*. (Note however that all formulae in this section are valid irrespective of whether or not the potentials overlap.)

We can write

$$G = G_a + G_a \left(\sum_{n \neq a} U_n \right) G \quad (2.13)$$

or, alternatively, the specular reflection of this:

$$G = G_a + G \left(\sum_{n \neq a} U_n \right) G_a \quad (2.14)$$

where G_a is the Green's function belonging to the potential U_a :

$$G_a = 1/(E + i\epsilon - K - U_a). \quad (2.15)$$

Substituting (2.14) in the right-hand side of (2.13) yields

$$G = G_a + G_a T_{aa} G_a \quad (2.16)$$

where

$$T_{aa} = \sum_{n \neq a} U_n + \left(\sum_{n \neq a} U_n \right) G \left(\sum_{m \neq a} U_m \right). \quad (2.17)$$

We finally obtain

$$\sigma_c = -\frac{F_1}{\pi} \sum_{m_i} \text{Im} \langle \psi_c | (H_I)_{10} [G_a + G_a T_{aa} G_a] (H_I)_{01} | \psi_c \rangle. \quad (2.18)$$

The first term in the RHS gives the total cross section for the photoemission from the isolated atom A. The second term represents all the contributions to σ_c due to single and multiple scatterings suffered by the photoelectron in the material.

The operator T_{aa} , if it were not for the fact that G also contains contributions from U_a , would represent the T -operator for the complete scattering of the photoelectron from the environment of the atom A. The multiple scatterings instead contain contributions from the reboundings of the photoelectron from the absorbing atom A also.

In order to evaluate T_{aa} , let us consider the operators T_{kj} defined as follows:

$$T_{kj} = \sum_{\substack{n \neq k \\ n \neq j}} U_n + \sum_{n \neq k} U_n G \sum_{m \neq j} U_m. \quad (2.19)$$

For $k = j = a$, T_{kj} reduces to T_{aa} . In (2.19), let us single out from G the contribution of the isolated atom N :

$$G = G_n + G_n \left(\sum_{p \neq n} U_p \right) G. \quad (2.20)$$

Using (2.20) in (2.19) we get

$$T_{kj} = \sum_{\substack{n \neq k \\ n \neq j}} U_n + \sum_{n \neq k} U_n G_n \sum_{m \neq j} U_m + \sum_{n \neq k} U_n G_n \sum_{p \neq n} U_p G \sum_{m \neq j} U_m. \quad (2.21)$$

Let us define the complete T -operator for the scattering of the photoelectron from the isolated atom N as t_n :

$$t_n = U_n + U_n G_n U_n. \quad (2.22)$$

We see that the first two terms in the RHS of (2.21) contain a sum of t_n s:

$$T_{kj} = \sum_{\substack{n \neq k \\ n \neq j}} t_n + \sum_{n \neq k} U_n G_n \left(\sum_{\substack{m \neq j \\ m \neq n}} U_m + \sum_{p \neq n} U_p G \sum_{m \neq j} U_m \right). \quad (2.23)$$

The bracket in the RHS of (2.23) is just T_{nj} , while for $U_n G_n$ we can use the identity

$$U_n G_n = t_n G_0 \quad (2.24)$$

where G_0 is the free-space Green's function:

$$G_0 = 1/(E + i\epsilon - K) \quad (2.25)$$

and G_n is linked to G_0 as usual by

$$G_n = G_0 + G_0 U_n G_n = G_0 + G_n U_n G_0.$$

We then get for T_{kj} a very simple integral equation:

$$T_{kj} = \sum_{\substack{n \neq k \\ n \neq j}} t_n + \sum_{n \neq k} t_n G_0 T_{nj} \quad (2.26)$$

Alternatively, one can easily see that the T s also satisfy the integral equation that is the specular reflection of (2.26):

$$T_{jk} = \sum_{\substack{n \neq k \\ n \neq j}} t_n + \sum_{n \neq k} T_{jn} G_0 t_n. \quad (2.27)$$

In the literature the following type of operators, called *scattering path operators* [55], have also been introduced:

$$\tau_{qp} = t_p \delta_{qp} + \sum_{m \neq q} t_q G_0 \tau_{mp} \quad \tau_{pq} = t_p \delta_{pq} + \sum_{m \neq q} \tau_{pm} G_0 t_q. \quad (2.28)$$

They are connected to our T_{kj} through the relation

$$T_{kj} = \sum_{\substack{q \neq k \\ p \neq j}} \tau_{qp}. \quad (2.29)$$

Introducing the second equation of (2.28) in the RHS of the first, we get

$$\tau_{qp} = t_p \delta_{qp} + t_q G_0 t_p (1 - \delta_{qp}) + t_q G_0 T_{qp} G_0 t_p \quad (2.30)$$

which for $p = q = a$ reads

$$\tau_{aa} = t_a + t_a G_0 T_{aa} G_0 t_a. \quad (2.31)$$

Finally, (2.31) can be inverted to find T_{aa} in terms of τ_{aa} :

$$T_{aa} = G_0^{-1} t_a^{-1} (\tau_{aa} - t_a) t_a^{-1} G_0^{-1}. \quad (2.32)$$

To find the analytic solution of the integral equations (2.26)–(2.28) is a rather formidable task. Formally, the solution of (2.28) is given by the matrix operator

$$\bar{\tau} = (1 - \Omega)^{-1} \vartheta \quad (2.33)$$

where the matrix operators $\bar{\tau}$, ϑ and Ω are defined according to

$$(\bar{\tau})_{qp} = \tau_{qp} \quad (\vartheta)_{qp} = t_p \delta_{qp} \quad (\Omega)_{qp} = t_q G_0 (1 - \delta_{qp}). \quad (2.34)$$

If $\|\Omega\Psi\| \ll \|\Psi\|$ for any normalizable vector Ψ of the combined scattering-state-atomic-site Hilbert space (we shall discuss this point again in section 5.3), then it is possible to expand $(1 - \Omega)^{-1}$ in the absolutely convergent geometric series:

$$\begin{aligned}\tilde{\tau} &= \sum_{n=0}^{\infty} \Omega^n \vartheta \\ \tau_{qp} &= t_p \delta_{qp} + t_q G_0 t_p (1 - \delta_{qp}) + t_q G_0 \sum_{\substack{m \neq p \\ m \neq q}} t_m G_0 t_p \\ &\quad + t_q G_0 \sum_{n \neq q} t_n G_0 \sum_{\substack{m \neq p \\ m \neq n}} t_m G_0 t_p + \dots\end{aligned}\quad (2.35)$$

The perturbative expansion (2.35) converges at high enough photoelectron energies, where the electron scattering is weak. Of course, wherever (2.35) fails to converge, the full solution (2.33) must be used.

We are now in the position to write down a perturbative expansion in multiple-scattering terms for T_{aa} . Just put the geometrical series (2.35) in (2.29):

$$\begin{aligned}T_{aa} &= \sum_{n \neq a} t_n + \sum_{n \neq a} t_n G_0 \sum_{\substack{m \neq n \\ m \neq a}} t_m + \sum_{n \neq a} t_n G_0 \sum_{m \neq n} t_m G_0 \sum_{\substack{k \neq m \\ k \neq a}} t_k \\ &\quad + \sum_{n \neq a} t_n G_0 \sum_{m \neq n} t_m G_0 \sum_{\substack{k \neq m \\ j \neq k \\ j \neq a}} t_j + \dots\end{aligned}\quad (2.36)$$

Using (2.36) in (2.18), we see that the generic term of the multiple-scattering expansion of the total cross section has the following closed-loop structure: after emission from the atom A, the complete (in the field U_a) propagator G_a takes the photoelectron to the atom J , the electron is scattered there (t_j) and gets propagated in free space (G_0) to the atom K ... until from the atom N the electron propagates, with the complete Green's function G_a , back to the atom A. Each leg of the closed-loop connects only different atoms. The atom A itself may appear as an intermediate step of a closed loop.

T_{aa} can be written as:

$$T_{aa} = \sum_{s=2}^{\infty} T_{aa}^{(s)} \quad (2.37)$$

where $T_{aa}^{(s)}$ is the contribution from an s -leg closed-loop, i.e. $s - 1$ rescatterings.

We have therefore obtained an expression of the total cross section as a sum of all the possible multiple scatterings. The overlap of these terms with that representing the photoemission from the isolated atom A gives rise to the structures (XANES and EXAFS) observed in the absorption coefficient.

Far above the threshold the scattering of the photoelectron is weak, so one can retain only the single-scattering term $s = 2$. At low electron energies, i.e. near the threshold, the scattering is strong; hence, in the energy region where the

perturbative expansion (2.35) still converges, one must also take into consideration multiple-scattering terms of higher order.

Before ending this section, we would like to point out that the operator T_{aa} , besides being the relevant operator for the description of all multiple scatterings in the absorption coefficient, is also responsible for taking into account these processes in the photoemission differential cross section since it appears in the T -matrix T_{f-i} .

In fact, let us introduce the scattering state $|\psi_f^{(-)(A)}\rangle$ from the isolated ionized atom A (Hamiltonian $K + U_a$). For the state vector $|\psi_f^{(-)}\rangle$ we can write

$$|\psi_f^{(-)}\rangle = |\psi_f^{(-)(A)}\rangle + G^{(-)} \sum_{n \neq a} U_n |\psi_f^{(-)(A)}\rangle \quad (2.38)$$

where $G^{(-)}$ is the incoming wave Green's function belonging to the (Hermitian) Hamiltonian H_f , which equals the Hermitian conjugate of G . The T -matrix (2.3) then reads as follows:

$$T_{f-i} = T_{f-i}^{(A)} + F_0 \langle \psi_f^{(-)(A)} | \sum_{n \neq a} U_n G(H_I)_{01} | \psi_c \rangle \quad (2.39)$$

where

$$T_{f-i}^{(A)} = F_0 \langle \psi_f^{(-)(A)} | (H_I)_{01} | \psi_c \rangle. \quad (2.40)$$

Introducing (2.14) for the complete Green's function G and using (2.17) we finally obtain

$$T_{f-i} = T_{f-i}^{(A)} + F_0 \langle \psi_f^{(-)(A)} | T_{aa} G_a(H_I)_{01} | \psi_c \rangle \quad (2.41)$$

which proves our statement.

3. The photoemission cross section and the multiple-scattering function $\chi_{L,L'}^\dagger$

We proceed to evaluate the total photoemission cross section σ_c . We now apply the dipole approximation, which amounts to substituting in (2.3) for $\langle 0 | H_I | 1_i \rangle \equiv (H_I)_{01}$ the quantity [72]†

$$(H_I)_{01} \rightarrow -i[\hbar\omega/2(2\pi)^3]^{1/2} \epsilon \cdot e \mathbf{r} \quad (3.1)$$

where ϵ is the unit polarization vector of the photon.

Equation (2.18) then reads

$$\sigma_c = -2\hbar\omega\alpha |F_0|^2 \sum_{m_i} \text{Im} \langle \psi_c | \epsilon \cdot \mathbf{r} [G_a + G_a T_{aa} G_a] \epsilon \cdot \mathbf{r} | \psi_c \rangle \quad (3.2)$$

† From now on we drop the subindex f from the final electron momentum $\hbar k_f$. The energy of the photon remains $\hbar\omega$. For the spherical harmonics we follow the notation of [82], appendix to chapter 2. In particular, the phase convention is: $Y_{l,m}^*(\mathbf{k}) = (-1)^m Y_{l,-m}(\mathbf{k})$. We shall use as much as possible the compound index $L \equiv (l, m)$.

‡ For a pure electric quadrupole transition, in the RHS of (3.1) replace $(\epsilon \cdot \mathbf{r})$ with $(i/2)(\mathbf{k}_{\text{photon}} \cdot \mathbf{r})(\epsilon \cdot \mathbf{r})$.

where $\alpha = e^2/\hbar c$. For $\epsilon \cdot \mathbf{r}|\psi_c\rangle$ we write

$$\epsilon \cdot \mathbf{r}|\psi_c\rangle = \frac{4\pi}{3} \sum_{m_1} Y_{1m_1}^*(\epsilon) Y_{1m_1}(\mathbf{r}) |Y_{L_1}\rangle |R_{L_1}\rangle. \quad (3.3)$$

We need now to evaluate the free G_0 and the complete G_a Green's functions. We shall use the notation $|\mathbf{r}\rangle_j$ for the eigenket of position used by the 'observer' J , i.e. the observer who has placed the origin of coordinates at the centre of the atom J .

For the free propagator we get (see pp 269, 298 of [83] where units $\hbar = 1$ are used):

$${}_a\langle \mathbf{r} | G_0 | \mathbf{r}' \rangle_a = -\frac{1}{4\pi} \frac{2m}{\hbar^2} \frac{e^{ik|\mathbf{r}-\mathbf{r}'|}}{|\mathbf{r}-\mathbf{r}'|} = \sum_L Y_L(\mathbf{r}) G_{0l}(r, r') Y_L^*(\mathbf{r}') \quad (3.4)$$

where

$$G_{0l}(r, r') = -ik(2m/\hbar^2) j_l(kr_<) h_l^{(+)}(kr_>). \quad (3.5)$$

$r_<$ indicates the smaller of r and r' , $r_>$ the larger. j_l , n_l and $h_l^{(+)} \equiv h_l^{(1)} = j_l + in_l = [h_l^{(2)}]^* \equiv [h_l^{(-)}]^*$ are the usual spherical Bessel, Neumann and Hankel functions (see [83], p 38, and [84], p 437).

For the complete propagator we get (see [83], p 374)

$$\begin{aligned} {}_a\langle \mathbf{r} | G_a | \mathbf{r}' \rangle_a &= \sum_L Y_L(\mathbf{r}) G_{al}(r, r') Y_L^*(\mathbf{r}') \\ G_{al}(r, r') &= -\frac{1}{4\pi} \frac{2m}{\hbar^2} \frac{(-i)^l}{kr r'} \psi_l^{(+)}(k, r_<) f_l^{(+)}(k, r_>). \end{aligned} \quad (3.6)$$

$\psi_l^{(+)}(k, r)$ is the physical wave function (note that our $\psi_l^{(+)}$ differs from that of [83]: $\psi_l^{(+)} = 4\pi \psi_l^{(+)(\text{Newton})}$) satisfying the boundary condition (regularity at the origin):

$$\lim_{r \rightarrow 0} (kr)^{-l-1} \psi_l^{(+)}(k, r) = 4\pi/[f_l(k)(2l+1)!!] \quad (3.7)$$

where $f_l(k)$ is the Jost function. $\psi_l^{(+)}(k, r)$ appears in the expansion of $\psi_f^{(+)}(k, r)$ in spherical harmonics:

$$\psi_f^{(+)}(k, r) = (2\pi)^{-3/2} \sum_{lm} Y_{lm}^*(\mathbf{k}) Y_{lm}(\mathbf{r}) i^l \frac{\psi_l^{(+)}(k, r)}{kr}. \quad (3.8)$$

Outside the radius R_{MT} of the muffin-tin potential, $\psi_f^{(+)}(k, r)$ is given by

$$\begin{aligned} \psi_f^{(+)}(k, r)_{r > R_{\text{MT}}} &= 4\pi k r \left[j_l(kr) + h_l^{(+)}(kr) i e^{i\delta_l^{(\text{A})}} \sin \delta_l^{(\text{A})} \right] \\ &= 4\pi k r e^{i\delta_l^{(\text{A})}} \left[j_l(kr) \cos \delta_l^{(\text{A})} - n_l(kr) \sin \delta_l^{(\text{A})} \right] \end{aligned} \quad (3.9)$$

where $\delta_l^{(A)}$ is the phase shift produced by the potential U_a of the relaxed ionized atom A. For large r (3.9) becomes

$$\psi_f^{(+)}(k, r) \underset{\text{large } r}{\approx} 2\pi i^{l+1} \left[e^{-ikr} + (-1)^{l+1} e^{ikr} e^{2i\delta_l^{(A)}} \right]. \quad (3.10)$$

From (2.5) one gets

$$\psi_l^{(-)}(k, r) = [\psi_l^{(+)}(k, r)]^* \quad (3.11)$$

and, using the fact that $f_l(k) = |f_l(k)| \exp(-i\delta_l^{(A)})$,

$$\psi_l^{(+)}(k, r) = e^{2i\delta_l^{(A)}} \psi_l^{(-)}(k, r). \quad (3.12)$$

$f_l^{(+)}(k, r)$ is an outgoing wave eigenfunction ($\neq \psi_l^{(+)}(k, r)$), which is irregular at the origin, determined by the boundary condition at infinity:

$$\lim_{r \rightarrow \infty} e^{-ikr} f_l^{(+)}(k, r) = 1. \quad (3.13)$$

Outside the potential $f_l^{(+)}(k, r)$ is just given by

$$f_l^{(+)}(k, r) \underset{r > R_{MT}}{=} i^{l+1} k r h_l^{(+)}(kr). \quad (3.14)$$

We now have all the elements that are necessary for computing σ_c . The cross section (3.2) is composed of two terms. Let us first evaluate the first one that describes the cross section $\sigma_c^{(A)}$ from the isolated atom A.

The cross section $\sigma_c^{(A)}$ can be obtained in a simpler way from (2.6), just substituting $T_{f-i}^{(A)}$ for T_{f-i} . The evaluation is straightforward and gives

$$\sigma_c^{(A)} = F_2 \sum_l \sum_{m_l} 4\pi \left(\sum_{m_i} (\langle Y_{1m_i} | Y_L Y_{L_i} \rangle)^2 \right) \frac{4\pi}{3} |Y_{1m_l}(\epsilon)|^2 M_l^{(A)} \quad (3.15)$$

where $F_2 = (\alpha m \omega / 12 \pi^2 \hbar k) |F_0|^2$ and $M_l^{(A)}$ is given by

$$M_l^{(A)} \equiv M_{l,l}^{(A)} \\ M_{l,l'}^{(A)} = \left(\int r dr \psi_l^{(-)*}(k, r) R_{l_l}(r) \right)^* \left(\int r' dr' \psi_{l'}^{(-)*}(k, r') R_{l_l}(r') \right). \quad (3.16)$$

In our notations, the (Gaunt) coefficients $\langle Y_L | Y_{L_1} Y_{L_2} \rangle$ are real. They are given by (use (A2.16) of [82])

$$\begin{aligned} \langle Y_L | Y_{L_1} Y_{L_2} \rangle &= \int d\Omega Y_L^*(\Omega) Y_{L_1}(\Omega) Y_{L_2}(\Omega) \\ &= \left[\frac{(2l_1 + 1)(2l_2 + 1)}{4\pi(2l + 1)} \right]^{1/2} C(l_1 l_2 l; m_1 m_2 m) C(l_1 l_2 l; 000). \end{aligned} \quad (3.17)$$

They vanish for $l + l_1 + l_2 = \text{odd}$. In order to evaluate the sum in large brackets appearing in (3.15), consider the quantity.

$$B_{LL'}(l_i, l_1) = \sum_{m_i, m_1} \langle Y_{l_i, m_i} Y_{l_1, m_1} | Y_{lm} \rangle \langle Y_{l', m'} | Y_{l_1, m_1} Y_{l_i, m_i} \rangle. \quad (3.18)$$

The calculation of (3.18) is standard [28]. Using (3.17) we obtain

$$B_{LL'}(l_i, l_1) = \frac{(2l_i + 1)(2l_1 + 1)}{4\pi[(2l + 1)(2l' + 1)]^{1/2}} C(l_i, l_1, l; 000) C(l_i, l_1, l'; 000) \\ \times \sum_{m_1} \sum_{m_i} C(l_i, l_1, l; m_i, m_1, m) C(l_i, l_1, l'; m_i, m_1, m'). \quad (3.19)$$

Here the sums over m_1 and m_i collapse to the value $\delta_{ll'} \delta_{mm'}$ due to completeness:

$$B_{LL'}(l_i, l_1) = \{(2l_i + 1)(2l_1 + 1)/[4\pi(2l + 1)]\} \delta_{LL'} [C(l_i, l_1, l; 000)]^2. \quad (3.20)$$

We see that (use the explicit expressions for the C -coefficients when one of the angular momenta is equal to 1, which can be found in table 2.3 of [82], appendix to ch 2):

$$\sum_{mm_i} ((Y_{1m_1} | Y_L Y_{L_i}))^2 \equiv B_{11}(l_i, l) = \frac{(2l_i + 1)(2l + 1)}{12\pi} [C(l_i, l, 1; 000)]^2 \\ = \frac{1}{4\pi} [(l_i + 1)\delta_{l, l_i+1} + l_i \delta_{l, l_i-1}]. \quad (3.21)$$

Finally, for the cross section $\sigma_c^{(A)}$ we get

$$\sigma_c^{(A)} = F_2 \sum_l [(l_i + 1)\delta_{l, l_i+1} + l_i \delta_{l, l_i-1}] \sum_{m_1} \frac{4\pi}{3} |Y_{1m_1}(\epsilon)|^2 M_l^{(A)}. \quad (3.22)$$

We would like to mention that in the literature use is often made of formulas simplified by choosing the polarization vector ϵ along the z -axis; in such a case one can write: $Y_{1m_1}(\epsilon) \equiv (3/4\pi)^{1/2} \delta_{m_1, 0}$.

Let us now evaluate the second term of (3.2), the one that contains all multiple-scattering contributions to the cross section. In these terms, G_a operates in expressions like $\langle A | G_a t_n \dots, n \neq a$, or the specular reflection of this. In our model of (non-overlapping) muffin-tin potentials, the physical wave function $\psi_i^{(+)}(k, r_<)$ entering $\langle r | G_a | r' \rangle$ will then be evaluated for $r_<$ lying inside the atom A , while $f_i^{(+)}(k, r)$ must be evaluated for $r_>$ inside the atom N . $r_>$ therefore being outside the muffin-tin region A , for $f_i^{(+)}(k, r)$ we can use (3.14).

Using (3.6), (3.11), (3.12) and (3.14) for the total photoemission cross section, we finally obtain

$$\sigma_c = F_2 \sum_{LL'} 4\pi \sum_{m_i, m_1, m'_1} \langle Y_{L_i} Y_{1m_1} | Y_L \rangle \langle Y_{L'} | Y_{1m'_1} Y_{L_i} \rangle \\ \times \text{Im} \left(\frac{4\pi}{3} Y_{1m_1}(\epsilon) Y_{1m'_1}^*(\epsilon) M_{l, l'}^{(A)} \chi_{L, L'} \right) \quad (3.23)$$

where the so-called *multiple-scattering function* $\chi_{L,L'}$ contains all the contributions from the environment of the absorbing atom:

$$\chi_{L,L'} = i\delta_{LL'} + \frac{2m}{\hbar^2} k e^{2i\delta_l^{(A)}} \times \int d^3r' d^3r''' Y_L^*(\mathbf{r}') h_l^{(+)}(kr') {}_a\langle \mathbf{r}' | T_{aa} | \mathbf{r}''' \rangle_a h_l^{(+)}(kr''') Y_{L'}(\mathbf{r}'''). \quad (3.24)$$

The first term in (3.24), i.e. $i\delta_{LL'}$, gives rise to the cross section $\sigma_c^{(A)\dagger}$.

We see that the multiple-scattering function $\chi_{L,L'}$ is nicely factorized in the expression for the total photoemission cross section. Also, from (2.37), we see that it can be written as a sum of contributions from the various multiple scatterings:

$$\chi_{L,L'} = i\delta_{LL'} + \sum_{s=2}^{\infty} \chi_{L,L'}^{(s)}. \quad (3.25)$$

To end this section, we give the expression for the total photoemission cross section averaged over the incoming photon polarization vector. In this case one gets that only the diagonal elements of the matrices $M^{(A)}$ and χ contribute. After the trivial angular integration, the quantity to be evaluated is $B_{LL'}(l_i, 1)$. From (3.20) we have

$$B_{LL'}(l_i, 1) = (3/4\pi) \delta_{LL'} [1/(2l+1)] [(l_i+1)\delta_{l,l_i+1} + l_i\delta_{l,l_i-1}]. \quad (3.26)$$

Hence the total photoemission cross section averaged over the polarization vector turns out to be

$$\bar{\sigma}_c \equiv \frac{1}{4\pi} \int_{4\pi} \sigma_c d\Omega_\epsilon = F_2 \sum_l [(l_i+1)\delta_{l,l_i+1} + l_i\delta_{l,l_i-1}] M_l^{(A)} \frac{1}{2l+1} \sum_m \text{Im } \chi_{L,L} \quad \text{unpolarized photon beam.} \quad (3.27)$$

The average of $\sigma_c^{(A)}$ is of course obtained from (3.27) by substituting 1 for $\text{Im } \chi_{L,L}$.

Finally, we note that the relation between the multiple-scattering function and the absorption coefficient (averaged over ϵ) is simplest for K-shell absorption. Using (3.27) with $l_i = 0$ we have

$$\frac{\bar{\mu}_c - \bar{\mu}_c^{(A)}}{\bar{\mu}_c^{(A)}} = \frac{1}{3} \sum_m \text{Im } \chi_{1m,1m} - 1 \quad (3.28)$$

where we have defined the isolated atom background as $\bar{\mu}_c^{(A)} \equiv n_c \bar{\sigma}_c^{(A)}$.

† An additional contribution to (3.24) arises when one has incomplete screening of the core-hole (non-metals and molecules). Instead of placing $V = 0$ beyond the last atom muffin-tin potential, one surrounds the cluster with the Coulomb tail originated by the core-hole [28, 57, 60]. Modifications to (3.24) must also be introduced when the interstitial potential cannot be approximated by a constant (as in the case of a charge density build-up along a bond) [56, 34].

4. The momentum space approach

We need now to evaluate the multiple-scattering function $\chi_{L,L'}^{(s)}$. We start in this section with an approximate approach which has the merit of giving a very simple and clear physical insight into the complicated problem of photoabsorption in condensed matter. I consider it of, so to speak, 'pedagogical' relevance. In its essence, it constitutes the finishing touch to the theories, set forth to explain this phenomenon, based on the so-called small-atom and plane-wave approximations (see section III of [14], and [23, 24]). The correct approach will be discussed in section 5.

The approach starts from the perturbative expansion (2.36). Therefore, even at the outset, we can say that it will be appropriate only at energies not too close to the edge. As we shall see, due to the muffin-tin structure of the potentials, all t -operators in (2.36) will appear evaluated on the energy shell.

Let us first take into consideration the role of the free-space Green's functions G_0 . The first term of (2.36) represents the contribution from single rescatterings, i.e. just one reflection from the environment (no G_0 there). All the other terms represent contributions from multiple scatterings. In these latter terms the free-space Green's function G_0 is always sandwiched between two t 's. Consider a typical grouping:

$$t_q G_0 t_p = \int d^3 r' \int d^3 r t_q |r'\rangle_p \langle r'| G_0 |r\rangle_p \langle r| t_p \quad q \neq p \quad (4.1)$$

where the propagator, ${}_p \langle r'| G_0 |r\rangle_p$ is given by (3.4). The operators t_p and t_q , standing of the right and left of G_0 , force r and r' to lie where the (non-overlapping) muffin-tin potentials U_p and U_q , respectively, do not vanish. Accordingly, we replace $|r - r'|$ in the denominator of (3.4) with the interatomic distance R_{qp} between atoms P and Q , while for the phase at the numerator of (3.4) we use the expansion

$$|r - r'| \equiv |\rho_p - \rho_q - R_{qp}| \cong R_{qp} - \rho \cdot R_{qp} / R_{qp} \quad (4.2)$$

where

$$R_{qp} = R_q - R_p \quad \rho_p = r \quad \rho_q = r' - R_{qp} \quad \rho = \rho_p - \rho_q. \quad (4.3)$$

This approximation is sensible to the extent that terms of the order of $(a/R_{qp})^2$, with $a < R_{MT}$, the radius of the core of the atom, can be neglected. We shall quote this as the *small-atom approximation*. Note that in (4.3) the vector ρ_j originates from the atom J and the vector R_{qp} points from atom P to atom Q , as shown in figure 1.

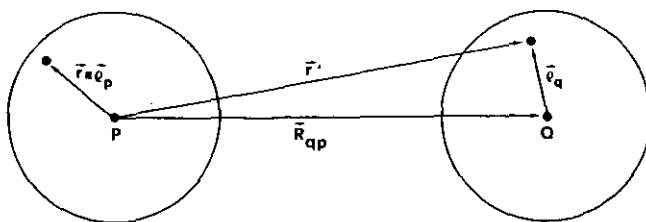


Figure 1. The vectors defining the Green's function in coordinate representation. r' joins the centre of the site P with the muffin-tin region $Q \neq P$. The Greek letter ρ always indicates a vector joining the centre of the site to a point within the same muffin-tin region.

Let us define the vector k_{qp} as

$$k_{qp} = kR_{qp}/R_{qp}. \quad (4.4)$$

Its modulus coincides with k while its direction is along the interatomic distance vector R_{qp} . For (4.1) we get

$$t_q G_0 t_p = \int d^3 \rho_q \int d^3 \rho_p t_q |\rho_q\rangle_q e^{ik_{qp} \cdot \rho_q} C S_{qp} e^{-ik_{qp} \cdot \rho_p} {}_p \langle \rho_p | t_p \quad q \neq p \quad (4.5)$$

where $C = -(m/2\pi\hbar^2)$ and we have defined a new electron propagation function:

$$S_{qp} = e^{ikR_{qp}}/R_{qp}. \quad (4.6)$$

In obtaining (4.5) we have used on the p -side the identity ${}_p \langle r | = {}_p \langle \rho_p |$ while on the q -side we have performed the substitution

$$|r'\rangle_p \Rightarrow |\rho_q\rangle_q. \quad (4.7)$$

This procedure is proved as follows. $|r'\rangle_p$ is used by the 'observer P '. If we want to relate the measurements of observer P with those performed by the 'observer Q ', we need to take a space translation of the displacement R_{pq} obtained by application of the unitary operator (see [82], ch 2.3)

$$D_{R_{qp}} = \exp(iP \cdot R_{qp}/\hbar) \quad (4.8)$$

where P is the total linear momentum of the system. We get

$$|r'\rangle_p = D_{R_{qp}}^\dagger |r' - R_{qp}\rangle_q \equiv D_{R_{qp}}^\dagger |\rho_q\rangle_q. \quad (4.9)$$

A moment reflection shows that substitutions of this type are performed once at each leg of the generic s -leg term of $\chi_{L,L'}^{(s)}$. Since P commutes with all the t_j -operators, in an s -leg term of $\chi_{L,L'}^{(s)}$ we can collect together the resulting s translation operators in the unique expression $\exp(-iP \cdot R/\hbar)$. But we are dealing only with closed loops, so for us $R = 0$ or $\exp(-iP \cdot R/\hbar) = 1$, and consequently the matrix element $\chi_{L,L'}^{(s)}$ is left invariant by the substitutions (4.7).

We now use the relation

$$e^{ik \cdot \rho_j} = (2\pi)^{3/2} {}_j \langle \rho_j | k \rangle \quad (4.10)$$

where $|k\rangle$ is eigenstate of the photoelectron momentum belonging to the eigenvalue $\hbar k$. Finally, using the completeness relations

$$\int d^3 \rho_j |\rho_j\rangle_j {}_j \langle \rho_j | = 1$$

equation (4.5) reads

$$t_q G_0 t_p = t_q |k_{qp}\rangle (2\pi)^3 C S_{qp} \langle k_{qp} | t_p \quad q \neq p. \quad (4.11)$$

Therefore, in the perturbative expansion (2.36), for a G_0 sandwiched between a t_q and a t_p , we can substitute the quantity

$$G_0 \Rightarrow (2\pi)^3 C S_{qp} \quad q \neq p \quad (4.12)$$

with S_{qp} given by (4.6).

For the t -operators there are three possibilities:

(i) t_p is sandwiched between two G_0 , as in the grouping $\dots t_q G_0 t_p G_0 t_m \dots$ ($q \neq p, p \neq m$);

(ii) t_p appears in a position like $\dots G_0 t_p |r'''\rangle_a, p \neq a$, or its specularly reflected expression;

(iii) t_p appears sandwiched between two eigenkets of position ${}_a\langle r' | t_p | r'''\rangle_a$.

Let us consider each of these cases in detail.

Case (i). As an application of (4.11), we trivially see that in a typical grouping of the type $\dots t_q G_0 t_p G_0 t_m \dots$ for t_p we can substitute the matrix

$$t_p \Rightarrow \langle k_{qp} | t_p | k_{pm} \rangle. \quad (4.13)$$

Reading from right to left, the t_p -matrix element $\langle k_{qp} | t_p | k_{pm} \rangle$ describes on the energy shell an electron which, having been shot from the atom M , gets scattered elastically from the target atom P with destination atom Q . The momentum of the electron is always directed along the vector joining the two atoms (k_{pm} before and k_{qp} after the collision with P) and its modulus is equal to k .

Case (ii). This occurs when t_p appears at the end or in front of T_{aa} . Consider then the resulting 'tail' of (3.24):

$$\dots t_q G_0 t_p \int d^3 r' |r'\rangle_a h_{l'}^{(+)}(kr') Y_{L'}(r') \quad (4.14)$$

which, using (4.11), reads

$$\dots t_q |k_{qp}\rangle (2\pi)^3 C S_{qp} \int d^3 r' \langle k_{qp} | t_p | r'\rangle_a h_{l'}^{(+)}(kr') Y_{L'}(r'). \quad (4.15)$$

In the evaluation of (4.15), we must develop $\langle k_{qp} | t_p | r'\rangle_a$ into a momentum space T -matrix on the energy shell.

First of all, we can substitute the matrix $\langle k_{qp} | t_p | \rho_p \rangle_p$ for $\langle k_{qp} | t_p | r'\rangle_a$ using (4.7). Secondly, the vector r' in (4.15) connects the centre of the atom A with the region where the muffin-tin potential U_p does not vanish. In the spirit of the small-atom approximation, we then substitute R_{pa} for r' in the argument of the spherical harmonic $Y_{L'}$. We then apply the so-called *plane-wave approximation* (PWA), which consists in taking the asymptotic expression of $h_{l'}^{(+)}(kr')$ for large kr' and writing $kr' \simeq k_{pa} \cdot r'$. We get (now $r' = \rho_p + R_{pa}$):

$$\begin{aligned} i^{l'+1} h_{l'}^{(+)}(kr') &\simeq e^{ikr'} / kr' \simeq e^{ik_{pa} \cdot r'} / k R_{pa} \\ &= e^{ik_{pa} \cdot \rho_p} e^{ik R_{pa}} / k R_{pa} \equiv (1/k) e^{ik_{pa} \cdot \rho_p} S_{pa}. \end{aligned} \quad (4.16)$$

Let us discuss the validity of the PWA for our case. Actually, the relevant quantity to consider, as a function of the energy, is the phase of the Hankel function. In fact, it is the phase that is responsible for the building up of the interference pattern observed in the absorption coefficient. We have (see [84], pp 439, 365) (here $z = kr'$):

$$\begin{aligned} i^{l'+1} h_{l'}^{(+)}(z) &= |\mathcal{M}_{l'}(z)| \exp[i\varphi_{l'}(z)] \\ \varphi_{l'}(z) &\approx z[1 + l'(l' + 1)/2z^2 + O(z^{-4})] \end{aligned} \quad (4.17)$$

$$|\mathcal{M}_{l'}(z)| \approx (1/z)[1 + l'(l' + 1)/2z^2 + O(z^{-4})]^{1/2}. \quad (4.18)$$

The second term in square brackets of (4.17) is bounded by (note that l' is fixed here: $l' = l_i \pm 1$):

$$l'(l' + 1)/(2z^2) < l'(l' + 1)/[2k^2(R_{pa} - R_{MT})^2].$$

This means that we can neglect the correction to the phase when

$$E \gg \hbar^2 l'(l' + 1)/[4m(R_{pa} - R_{MT})^2]. \quad (4.19)$$

Equation (4.19) defines the energy range of validity of the PWA. Below the energy defined by (4.19), our momentum approach fails and one must resort to the correct curved-wave theory of section 5.

Use of (4.16) in (4.14) gives

$$\dots t_q |k_{qp}\rangle (2\pi)^3 C S_{qp} \int d^3 \rho_p \langle k_{qp} | t_p | \rho_p \rangle_p e^{i\mathbf{k}_{pa} \cdot \boldsymbol{\rho}_p} k^{-1} S_{pa}(-i)^{l'+1} Y_{L'}(\mathbf{R}_{pa}).$$

Using now (4.7) and the completeness of the set of eigenkets of position $\{|\rho_p\rangle_p\}$, we finally get for (4.14), i.e. for the 'tail' of (3.24),

$$\dots (-i) t_q |k_{qp}\rangle (2\pi)^3 C S_{qp} \langle k_{qp} | t_p | k_{pa} \rangle S_{pa} (2\pi)^{3/2} k^{-1} [(-i)^{l'} Y_{L'}(\mathbf{R}_{pa})] \quad (4.20)$$

and similarly for the corresponding 'front' of (3.24)

$$(-i) [Y_L(\mathbf{R}_{ap}) (-i)^{l'}]^* k^{-1} (2\pi)^{3/2} S_{ap} \langle k_{ap} | t_p | k_{pq} \rangle (2\pi)^3 C S_{pq} \langle k_{pq} | t_q \dots \quad (4.21)$$

where we have used the fact that: $Y_L(-\mathbf{R}) = (-)^l Y_L(\mathbf{R})$.

Case (iii). This is the case of a single scattering of the photoelectron from the atoms surrounding the absorbing atom A. Using the very same procedures as above, we immediately get

$$\begin{aligned} & \int d^3 r' \int d^3 r''' Y_L^*(\mathbf{r}') h_l^{(+)}(k r')_a \langle \mathbf{r}' | t_p | \mathbf{r}''' \rangle_a h_l^{(+)}(k r''') Y_{L'}(\mathbf{r}''') \\ &= - [(-i)^l Y_L(\mathbf{R}_{ap})]^* k^{-1} (2\pi)^{3/2} S_{ap} \langle k_{ap} | t_p | k_{pa} \rangle \\ & \quad \times S_{pa} (2\pi)^{3/2} k^{-1} [(-i)^{l'} Y_{L'}(\mathbf{R}_{pa})]. \end{aligned} \quad (4.22)$$

By collecting the various results obtained, we see that the structure of the multiple-scattering term $\chi_{L,L'}^{(s)}$, representing the generic s -leg closed loop is very simple: we get a sequence of s free electron propagators S_{k_j} with $s - 1$ interaction matrix elements $\langle k_{r_q} | t_q | k_{qp} \rangle$ interposed in between them.

It is convenient to introduce the scattering amplitude f_q defined through the momentum space t_q -matrix on the energy shell:

$$\langle k_{r_q} | t_q | k_{qp} \rangle \equiv -(1/m)(\hbar/2\pi)^2 f_q(\vartheta_{rqp}) \quad (4.23)$$

where ϑ_{rqp} , the angle formed by the vectors k_{r_q} and k_{qp} , represents the co-latitude angle of scattering from the site Q . The scattering amplitude does not depend on the azimuthal angle since our muffin-tin potentials have been supposed to be spherically symmetric. The squared modulus of the scattering amplitude f_q is exactly equal to

the differential cross section for the elastic scattering of the photoelectron from the atom Q :

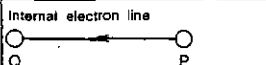
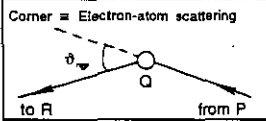
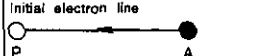
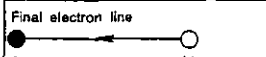
$$d\sigma/d\Omega = |f(\vartheta)|^2. \quad (4.24)$$

In terms of phase shifts, $f(\vartheta)$ is given by

$$f(\vartheta) = \sum_L Y_L^*(\mathbf{k}_f) \frac{4\pi}{k} e^{i\delta_l} \sin \delta_l Y_L(\mathbf{k}_i) = \frac{1}{k} \sum_l (2l+1) P_l(\cos \vartheta) e^{i\delta_l} \sin \delta_l. \quad (4.25)$$

The general form of the multiple-scattering function $\chi_{L,L'}^{(s)}$ can then be best understood in graphical form. We represent one term of $\chi_{L,L'}^{(s)}$ with a closed-loop s -leg diagram in which a *line* corresponds to the free propagation of the electron from an atom to the next and a *corner* stands for the scattering of the electron from an atom. The factor in front of the s -leg diagram (see (3.24)) includes $(2m/\hbar^2)k \exp(2i\delta_l^{(A)})$ where $\exp(2i\delta_l^{(A)})$ is of course representative of the scattering of the photoelectron from the potential U_a of the ionized atom A . The initial and final legs (see (4.20)–(4.21)) contribute $(-1)(2\pi)^3 k^{-2} [(-i)^l Y_L(\mathbf{R}_{av})]^* [(-i)^{l'} Y_{L'}(\mathbf{R}_{pa})]$; the other $s-2$ propagators give $[(2\pi)^3 C]^{s-2}$ while the $s-1$ transformations $t_q \rightarrow f_q$ yield a factor $[-\hbar^2/(4\pi^2 m)]^{s-1}$. Collecting all the results, we finally obtain the rules to construct a generic closed-loop diagram as shown in table 1.

Table 1. Correspondence between diagrams and multiple-scattering terms in the (approximate) momentum space approach.

Component of Diagram	Factor in $\chi_{L,L'}^{(s)}$
	$S_{qp} \equiv \frac{e^{i\delta_{qp}}}{R_{qp}}$
	$f_q(\vartheta_{qp})$
	$S_{pa} [(-i)^l Y_L(\mathbf{R}_{pa})]$
	$\frac{4\pi}{k} e^{2i\delta_l^{(A)}} [(-i)^{l'} Y_{L'}(\mathbf{R}_{va})]^* S_{av}$
<p>Each diagram is a closed-loop starting from the atom A. There are $s-2$ internal lines and $s-1$ corners (A is not a corner). In order to get the complete $\chi_{L,L'}^{(s)}$ one must sum on all the closed-loops of same order s.</p> <p>Note that each diagram must still be corrected for the effect of inelasticities and disorder (see Sect.5.2).</p>	

Using the recipes given in table 1, we can easily write down the multiple-scattering function for the generic closed-loop diagram $A, P, Q, R, \dots, T, U, V, A$ (read equations from right to left!):

$$\begin{aligned} \chi_{L,L'}^{(s)} = & \frac{4\pi}{k} \sum_{\text{loops}} e^{2i\delta_l^{(A)}} [(-i)^l Y_L(\mathbf{R}_{av})]^* S_{av} f_v(\vartheta_{avu}) S_{vu} f_u(\vartheta_{vut}) S_{ut} \dots \\ & \dots S_{rq} f_q(\vartheta_{rqp}) S_{qp} f_p(\vartheta_{qpa}) S_{pa} [(-i)^{l'} Y_{L'}(\mathbf{R}_{pa})]. \end{aligned} \quad (4.26)$$

This s -leg term is characterized by the propagator's contribution

$$e^{ikR_{\text{tot}}}/R_1 R_2 \dots R_s \quad R_{\text{tot}} \equiv R_1 + R_2 + \dots + R_s. \quad (4.27)$$

If we Fourier transform (4.26) on the momentum k , we see that the transformed s -leg amplitude

$$\tilde{\chi}_{LL'}^{(s)}(\tau) = \frac{1}{(2\pi)^{1/2}} \int dk \exp(-ikr) \chi_{LL'}^{(s)}(k) \quad (4.28)$$

will peak close to $r = R_{\text{tot}} \equiv \text{total closed-loop length}$ (the exact position of the peak depends of course also on the other energy-dependent factors present in (4.26)). This is the first information that one can obtain from (4.26). Another general consideration is the following: take (3.27), i.e. the average over the polarization vector. The angular factors in (4.26) yield

$$\frac{1}{2l+1} \sum_m Y_L^*(\mathbf{R}_{av}) Y_L(\mathbf{R}_{pa}) = \frac{1}{4\pi} P_l(\cos \vartheta_{vap})$$

where, in our notation, $\pi - \vartheta_{vap}$ is the angle under which A 'sees' the atoms P and V . In particular, for K-edge absorption we have a vanishing of the amplitude χ_{LL} when this angle is $\pi/2$.

Let us consider in some more detail the cases $s = 2, 3, 4$.

Single-scattering case $s = 2$: the traditional EXAFS. The diagram is shown in figure 2. It consists of only two electron lines (an initial and a final one) and one corner. We get

$$\chi_{L,L'}^{(2)} = \frac{4\pi}{k} e^{2i\delta_l^{(A)}} \sum_{p \neq a} [(-i)^l Y_L(\mathbf{R}_{ap})]^* S_{ap} f_p(\vartheta_{apa}) S_{pa} [(-i)^{l'} Y_{L'}(\mathbf{R}_{pa})]. \quad (4.29)$$

Since $\vartheta_{apa} = \pi$, the relevant amplitude f_p is evaluated at the backscattering angle π .

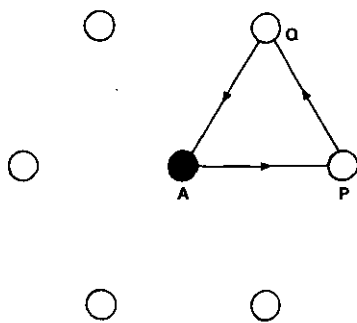
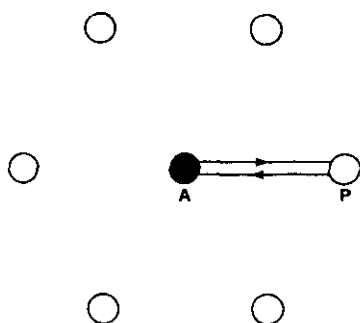


Figure 2. A closed-loop diagram for $s = 2$ (EXAFS). Figure 3. A closed-loop diagram for $s = 3$.

Let us see the expression one gets for absorption from a K shell. In that case we have $l_i = 0$, so $l = l' = 1$. Taking the polarization vector along the z -axis for simplicity we also have $m = m' = 0$. We get

$$\text{Im } \chi_{10,10}^{(2)(\text{K edge})} = -3 \sum_{p \neq a} \left(\epsilon \cdot \frac{\mathbf{R}_{pa}}{R_{pa}} \right)^2 \frac{|f_p(\pi)|}{k R_{pa}^2} \sin(2k R_{pa} + 2\delta_1^{(\Lambda)} + \Phi_p) \quad (4.30)$$

where for the backscattering amplitude $f_p(\pi)$ we have written

$$f_p(\pi) = |f_p(\pi)| \exp(i\Phi_p). \quad (4.31)$$

Obviously, the p th term of (4.30) vanishes when the angle between the bond direction \mathbf{R}_{pa} and the polarization angle ϵ is $\pi/2$.

For unpolarized photons, using (4.29) and (3.27), we get:

$$\frac{1}{2l+1} \sum_m \text{Im } \chi_{LL}^{(2)} = (-1)^l \sum_i \frac{N_i |f_i(\pi)|}{k R_i^2} \sin(2k R_i + 2\delta_l^{(\Lambda)} + \Phi_i) \quad (4.32)$$

unpolarized photon beam

where N_i is the number of identical atoms on the i th shell at the distance R_i from the absorber (coordination number). With due changes to take into account the effect of inelasticities and disorder, which we shall treat in section 5, equations (4.30), (4.32) have been the most used in applications.

The double- and triple-scattering cases $s = 3, 4$. Let us now write down the expressions for $\chi_{L,L'}^{(3)}$ and $\chi_{L,L'}^{(4)}$ that involve two and three scatterings, respectively, from the environment of the absorbing atom A, and which then contain information on second- and third-nearest-neighbour distances from A. The diagrams to be considered in these cases are shown in figures 3 and 4. Using the recipes of table 1 we easily get

$$\begin{aligned} \chi_{L,L'}^{(3)} = & \frac{4\pi}{k} \sum_{q \neq a} \sum_{\substack{p \neq a \\ p \neq q}} e^{2i\delta_l^{(\Lambda)}} [(-i)^l Y_L(\mathbf{R}_{aq})]^* S_{aq} f_q(\vartheta_{aqp}) \\ & \times S_{qp} f_p(\vartheta_{qpa}) S_{pa} [(-i)^{l'} Y_{L'}(\mathbf{R}_{pa})] \end{aligned} \quad (4.33)$$

$$\begin{aligned} \chi_{L,L'}^{(4)} = & \frac{4\pi}{k} \sum_{t \neq a} \sum_{q \neq t} \sum_{\substack{p \neq q \\ p \neq a}} e^{2i\delta_l^{(\Lambda)}} [(-i)^l Y_L(\mathbf{R}_{at})]^* S_{at} f_t(\vartheta_{atq}) \\ & \times S_{tq} f_q(\vartheta_{tqp}) S_{qp} f_p(\vartheta_{qpa}) S_{pa} [(-i)^{l'} Y_{L'}(\mathbf{R}_{pa})]. \end{aligned} \quad (4.34)$$

$\chi_{L,L'}^{(3)}$ gives a correlation of three atoms in space. Therefore, even though it is in general smaller than the single-scattering contribution (it involves a longer distance travelled by the photoelectron and finite-angle weak scatterings (see for example [14],

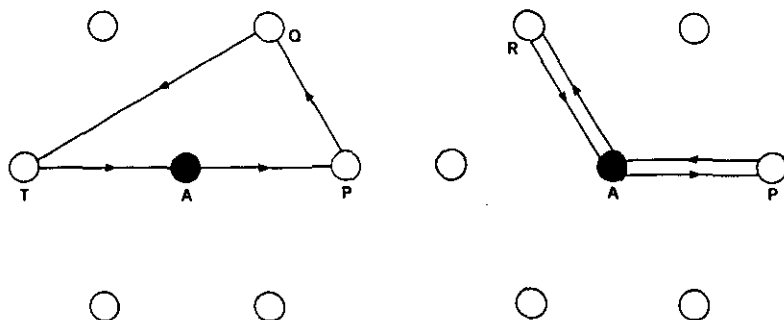


Figure 4. Closed-loop diagram for $s = 4$.

figure 5)), it provides us with the possibility of measuring, for example, the bond angle ϑ_{qap} under which the atom A sees atoms P and Q [23, 27, 41].

In the case of $\chi_{L,L'}^{(4)}$, we also have the possibility, shown in the second diagram of figure 4, in which the absorber A appears as an intermediate step of the closed loop.

The EXAFS spectra get enhanced when two scatterers are in alignment with the absorber A, an effect quoted as 'shadowing' in the literature [14]. This is, e.g., the case of FCC lattice structures. The relevant diagrams are shown in figure 5. The total contribution $\chi^{(\text{shadow})} \equiv \chi^{(2)} + \chi^{(3)} + \chi^{(4)}$ of these diagrams is given by

$$\chi_{L,L'}^{(\text{shadow})} = \frac{4\pi}{k} e^{2i\delta_l^{(A)}} [(-i)^l Y_L(R_{aq})]^* f_q(\pi) e^{2ikR_{aq}} \\ \times \left(\frac{1}{R_{aq}} + \frac{1}{R_{ap}} f(0) \frac{1}{R_{pq}} \right)^2 [(-i)^{l'} Y_{L'}(R_{pa})]. \quad (4.35)$$

The enhancement comes from the fact that the electron-atom scattering amplitude at forward angles $f(0)$ may be quite large. The result is that the amplitude of the wave coming in to the atom Q, after being scattered from the collinear atom P, can be larger than that of the wave that has experienced no scattering from P. A focusing effect occurs and the global contribution $\chi^{(3)} + \chi^{(4)}$ of these multiple scatterings dominates over the contribution $\chi^{(2)}$ of the single scattering from the shell that the atom Q belongs to.

Equations (4.33) and (4.34) contain information on XANES, the structure appearing in the absorption coefficient at low photoelectron energy. However, the approach of this section fails at low energies (see (4.19)) and a discussion on this point must be performed in the framework of the correct curved-wave theory of section 5 and its full (non-perturbative) solution.

5. The curved-wave theory

We now review (section 5.1) the correct approach to multiple scattering, which will be called *curved-wave theory* [8, 13, 14, 25, 29]. In section 5.2 consideration will be given to the treatment of inelasticities and disorder. In section 5.3 the full solution will be discussed.

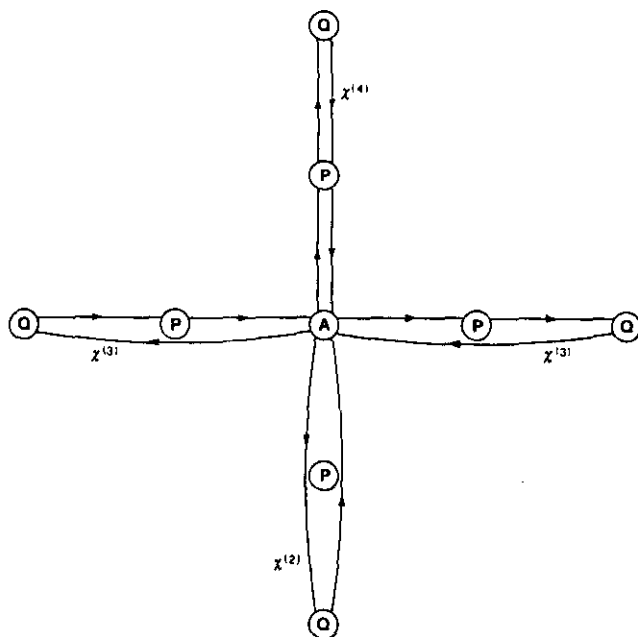


Figure 5. The shadowing effect.

5.1. The formalism in angular momentum space

The formalism must be developed in the angular momentum representation. We shall obtain a final formula for (3.24) where all the t_p -matrix elements contained in T_{aa} will be written in the form

$${}_p \langle j_l Y_L | t_p | j_{l'} Y_{L'} \rangle_p. \quad (5.1)$$

They will all appear evaluated on the energy shell, since the muffin-tin potentials occupy disjoint regions of space with constant interstitial potential. The state $|j_l Y_L\rangle_p$ is defined, for fixed klm , relative to the site P . It is the product of a spherical harmonic (with angles originating from P), and a spherical (regular in P) Bessel function. Its coordinate representation is†

$$\langle \mathbf{r} | j_l Y_L \rangle = j_l(kr) Y_L(\mathbf{r}). \quad (5.2)$$

We must transform all waves of the type $h_l^{(+)} Y_L$, outgoing from the site P (and therefore singular in P), in waves of the type (5.2) converging to the site Q (and regular there). This is readily done by using the expansion in angular momentum

† The normalization and momentum representation of these states are

$$\langle j_l(\mathbf{k}) Y_L | j_{l'}(\mathbf{k}') Y_{L'} \rangle = \frac{\pi}{2} \delta_{LL'} \frac{\delta(\mathbf{k} - \mathbf{k}')}{k^2} \quad \langle \mathbf{k}' | j_l(\mathbf{k}) Y_L \rangle = \left(\frac{\pi}{2}\right)^{1/2} i^{-l} Y_L(\mathbf{k}') \frac{\delta(\mathbf{k} - \mathbf{k}')}{k^2}.$$

space of the free Green's function (as usual, the limit $\epsilon \rightarrow 0^+$ is understood):

$$\begin{aligned} {}_p\langle r|G_0|r'\rangle_p &= -\frac{2m}{\hbar^2} \frac{1}{(2\pi)^3} \int \frac{d^3k'}{k'^2 - k^2 - i\epsilon} e^{ik'\cdot R_{pq}} e^{ik'\cdot \rho_p} e^{-ik'\cdot \rho_q} \\ &= -\frac{16m}{\hbar^2} \sum_{L_p L_q} i^{l+l_p-l_q} \langle Y_{L_p} Y_L | Y_{L_q} \rangle Y_{L_p}(\rho_p) Y_L(R_{pq}) Y_{L_q}^*(\rho_q) J(k) \end{aligned} \quad (5.3)$$

where the integral $J(k)$ is given by

$$J(k) = \int_0^\infty \frac{k'^2 dk'}{k'^2 - k^2 - i\epsilon} j_l(k' R_{qp}) j_{l_q}(k' \rho_q) j_{l_p}(k' \rho_p). \quad (5.4)$$

$J(k)$ can be integrated in the complex k' -plane. We shall do this supposing $\rho_p \equiv r < r' \equiv |R_{qp} + \rho_q|$ which, in our model of non-overlapping muffin-tin potentials, means $\rho_p + \rho_q < R_{qp}$.

For the Bessel function j_l we write $j_l = (h_l^{(+)} + h_l^{(-)})/2$. We next transform the part of the integral containing $h_l^{(-)}$ into an integral over the real negative k' -axis using the reflection properties $j_l(-z) = (-)^l j_l(z)$, $h_l^{(-)}(-z) = (-)^l h_l^{(+)}(z)$. We get

$$J(k) = \frac{1}{2} \left(\int_0^\infty + (-1)^{l+l_q+l_p} \int_{-\infty}^0 \right) \frac{k'^2 dk'}{k'^2 - k^2 - i\epsilon} h_l^{(+)} j_{l_q} j_{l_p}. \quad (5.5)$$

$J(k)$ in (5.3) is actually multiplied by the Gaunt coefficient $\langle Y_{L_p} Y_L | Y_{L_q} \rangle$ which is non-vanishing only if $l + l_p + l_q = \text{even}$. We therefore obtain

$$J(k) = \frac{1}{2} \int_{-\infty}^{+\infty} \frac{k'^2 dk'}{k'^2 - k^2 - i\epsilon} h_l^{(+)} j_{l_q} j_{l_p}. \quad (5.6)$$

We can perform the integral (5.6) in the complex k' -plane by closing the integration contour with an asymptotic semicircle in the upper half k' -plane, where $h_l^{(+)} j_{l_q} j_{l_p}$ vanish exponentially because of the condition $\rho_p + \rho_q < R_{qp}$. We get

$$J(k) = (i/2) \pi k h_l^{(+)}(k R_{qp}) j_{l_q}(k \rho_q) j_{l_p}(k \rho_p). \quad (5.7)$$

For the free Green's function we finally obtain

$$\begin{aligned} {}_p\langle r|G_0|r'\rangle_p &= k \frac{2m}{\hbar^2} \sum_{L_p L_q} j_{l_p}(k \rho_p) Y_{L_p}(\rho_p) g_{L_p L_q}(R_p - R_q) \\ &\quad \times \left[j_{l_q}(k \rho_q) Y_{L_q}(\rho_q) \right]^* \quad \rho_p + \rho_q < R_{pq} \end{aligned} \quad (5.8)$$

where the propagator g is given by

$$g_{L_p L_q}(R_{pq}) = -i \sum_L 4\pi i^{l+l_p-l_q} \langle Y_{L_p} Y_L | Y_{L_q} \rangle Y_L(R_{pq}) h_l^{(+)}(k R_{pq}). \quad (5.9)$$

Comparing this expression with (3.4), (3.5) evaluated for $r < r'$ and identifying the terms of the expansion in $Y_{L_p}(\rho_p)$, we get the expansion of the wave $h_l^{(+)} Y_L^*$:

$$h_l^{(+)}(kr') Y_{L_p}^*(r') = \sum_{L_q} i g_{L_p L_q}(\mathbf{R}_{pq}) j_{l_q}(k\rho_q) Y_{L_q}^*(\rho_q) \quad \rho_q < R_{pq}. \quad (5.10)$$

Taking the complex conjugate of (5.10) and exchanging k into $-k$, we get also the expansion of the wave $h_l^{(+)} Y_L$:

$$h_l^{(+)}(kr') Y_{L_p}(r') = \sum_{L_q} j_{l_q}(k\rho_q) Y_{L_q}(\rho_q) i g_{L_q L_p}(\mathbf{R}_{qp}) \quad \rho_q < R_{pq}. \quad (5.11)$$

Equations (5.10), (5.11) yield the desired expansion of the wave outgoing from the site P in terms of waves coming in to the site Q . Let us now construct the multiple-scattering function $\chi_{L_p L'}$ following the lines of thought in section 4.

For the free Green's function, using (5.8), we have

$$t_q G_0 t_p = k \frac{2m}{\hbar^2} t_q \sum_{L_p L_q} |j_{l_q} Y_{L_q}\rangle_q g_{L_q L_p}(\mathbf{R}_{qp})_p \langle j_{l_p} Y_{L_p} | t_p. \quad (5.12)$$

Let us now discuss the t -operators.

Case (i). t_p is sandwiched between two G_0 as in the grouping $\dots t_q G_0 t_p G_0 t_m \dots$. As an application of (5.12), we immediately see that for t_p we can substitute the on-energy shell matrix element:

$$t_p \Rightarrow {}_p \langle j_{l_p} Y_{L_p} | t_p | j_{l_p} Y_{L_p} \rangle_p. \quad (5.13)$$

Case (ii). This is the case when t_p appears at the 'tail' or in 'front' of (3.24). Using (5.10), (5.11) and (4.7) we easily get

$$\dots \int d^3 r''' t_p |r'''\rangle_a h_l^{(+)}(kr''') Y_{L'}(r''') = \dots \sum_{L_p} t_p |j_{l_p} Y_{L_p}\rangle_p i g_{L_p L'}(\mathbf{R}_{pa}) \quad (5.14)$$

$$\int d^3 r' Y_L^*(r') h_l^{(+)}(kr') \langle r' | t_p \dots = \sum_{L_p} i g_{L L_p}(\mathbf{R}_{ap})_p \langle j_{l_p} Y_{L_p} | t_p \dots \quad (5.15)$$

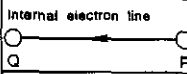
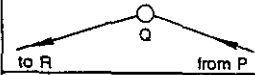
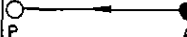
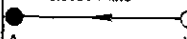
Case (iii). In this case one considers the term (3.24), treating only one rescattering from the environment. Use of (5.10), (5.11) and (4.7) gives immediately

$$\begin{aligned} & \int d^3 r' d^3 r''' Y_L^*(r') h_l^{(+)}(kr') \langle r' | t_p | r'''\rangle_a h_{l'}^{(+)}(kr''') Y_{L'}(r''') \\ &= - \sum_{L_p L'_p} g_{L L_p}(\mathbf{R}_{ap})_p \langle j_{l_p} Y_{L_p} | t_p | j_{l'_p} Y_{L'_p} \rangle_p g_{L'_p L'}(\mathbf{R}_{pa}). \end{aligned} \quad (5.16)$$

In order to write down the generic matrix element of (3.24), we redefine the on-shell t -matrix elements. Because of the spherical symmetry we can write

$$\langle k | t_p | k' \rangle = \sum_L Y_L^*(k) \frac{\hbar^2}{\pi m k} t_l^p Y_L(k') \quad (5.17)$$

Table 2. Correspondence between diagrams and multiple-scattering terms in the (exact) curved-wave theory.

Component of Diagram	Factor in $\chi_{LL'}^{(s)}$
Internal electron line 	$g_{L_q L_p}(\vec{R}_q - \vec{R}_p)$
Corner ■ Electron-atom scattering 	$t_q^s = -\exp(i\delta_{l_q}^{(q)}) \sin \delta_{l_q}^{(q)}$
Initial electron line 	$g_{L_q L}(\vec{R}_p - \vec{R}_s)$
Final electron line 	$-\exp(2i\delta_{l_q}^{(A)}) g_{L L'}(\vec{R}_s - \vec{R}_{s'})$
Each diagram is a closed-loop starting from the atom A. There are $s-2$ internal lines and $s-1$ corners (A is not a corner). In order to get a given s -leg term of $\chi_{LL'}^{(s)}$, one must sum over all intermediate angular momenta. The complete $\chi_{LL'}^{(s)}$ is obtained by summing all the closed-loops of same order s . Note that each diagram must still be corrected for the effect of inelasticities and disorder (see Sect.5.2).	

which means

$${}_p \langle j_l Y_L | t_p | j_{l'} Y_{L'} \rangle_p = \delta_{LL'} (\hbar^2/2m) (1/k) t_l^p \quad (5.18)$$

with t_l^p given by

$$t_l^p = -e^{i\delta_{l'}^{(p)}} \sin \delta_{l'}^{(p)}. \quad (5.19)$$

Introducing diagrams again, by collecting the results (5.12)–(5.19), we obtain the very simple rules shown in table 2 for the construction of an s -leg diagram.

The multiple-scattering function $\chi_{L,L'}$ has then the form

$$\chi_{L,L'} = i\delta_{LL'} - \sum_{\substack{q \neq a \\ p \neq a}} \sum_{L_q L_p} e^{2i\delta_{l_q}^{(A)}} [g_{LL_q}(\mathbf{R}_{aq})] \tau_{L_q L_p}^{qp} [g_{L_p L'}(\mathbf{R}_{pa})] \quad (5.20)$$

or, using (5.19) for the site A, the alternative expression

$$\chi_{L,L'} = i\delta_{LL'} - \left[e^{i(\delta_{l_q}^{(A)} - \delta_{l'}^{(A)})} / (\sin \delta_{l_q}^{(A)} \sin \delta_{l'}^{(A)}) \right] (\tau_{LL'}^{aa} - t_{l_q}^a \delta_{LL'}). \quad (5.21)$$

$\tau_{L_q L_p}^{qp}$ is given by the expansion

$$\begin{aligned} \tau_{L_q L_p}^{qp} &= t_{l_p}^p \delta_{qp} \delta_{L_q L_p} + t_{l_q}^q [g_{L_q L_p}(\mathbf{R}_{qp})] t_{l_p}^p (1 - \delta_{qp}) \\ &+ \sum_{\substack{m \neq q \\ m \neq p}} t_{l_q}^q [g_{L_q L_m}(\mathbf{R}_{qm})] t_{l_m}^m [g_{L_m L_p}(\mathbf{R}_{mp})] t_{l_p}^p + \dots \end{aligned} \quad (5.22)$$

The operator $\tau_{L_q L_p}^{qp}$ appearing in (5.20)–(5.22) is more useful, for computational purposes, than the operator T_{aa} of (3.24), since, unlike T_{aa} , its subindices qp actually refer to single-site t -operators, one (t^q) standing to the left and one (t^p) to the right of its expression.

The perturbative expansion (5.22) is to be compared with the expansion obtained in the (approximate) momentum space approach, of which (4.26) is the generic s -term. We see that, even though expressions (5.20)–(5.22) are simple, their physical content is more obscure due to the more complicated structure of the g -propagators as compared with the S -propagators. Therefore, the momentum space approach is more useful when one wants to reach a simple understanding of the phenomenon of x-ray absorption in condensed systems. In contrast, if one wishes to compare (in the framework of the considered single-particle formulation combined with dipole approximation and (elastic) muffin-tin potentials) theory correctly with experiment, one must resort to the so-called curved-wave approach (5.20)–(5.22).

Let us consider in detail the case of single scattering when the average over the polarization vector \mathbf{e} is performed. Using (5.20) with $\tau_{L_q L_p}^{qp} = t_{l_p}^p \delta_{qp} \delta_{L_q L_p}$ and the explicit expression (5.9) for the g -propagators, we get

$$\frac{1}{2l+1} \sum_m \text{Im} \chi_{L,L}^{(2)} = \frac{(4\pi)^2}{2l+1} \sum_{p \neq a} \text{Im} \left(e^{2i\delta_l^{(A)}} \sum_{L_1 L_2} Y_{L_1}^*(\mathbf{R}_{pa}) Y_{L_2}(\mathbf{R}_{ap}) i^{l_1+l_2} \right. \\ \left. \times h_{l_1}^{(+)}(kR_{pa}) h_{l_2}^{(+)}(kR_{pa}) \sum_{l_p} t_{l_p}^p B_{L_1 L_2}(l, l_p) \right). \quad (5.23)$$

Using now (3.20) and the fact that

$$\sum_m Y_L^*(\mathbf{r}) Y_L(-\mathbf{r}) = \frac{2l+1}{4\pi} (-1)^l$$

we obtain the exact curved-wave single-scattering formula:

$$\frac{1}{2l+1} \sum_m \text{Im} \chi_{L,L}^{(2)} = \sum_{p \neq a} \text{Im} \left\{ e^{2i\delta_l^{(A)}} \sum_{l_p} (2l_p+1) t_{l_p}^p H_p(l, l_p) \right\} \quad (5.24)$$

where $t_{l_p}^p$ is given by (5.19) and $H_p(l, l_p)$ by

$$H_p(l, l_p) = \sum_{l_1} \left[h_{l_1}^{(+)}(kR_{pa}) C(l l_p l_1; 000) \right]^2. \quad (5.25)$$

From the exact expression (5.24) we can reobtain the approximate EXAFS formula (4.32). We just use the PWA for the Hankel function appearing in (5.25): $i^{l_1+1} h_{l_1}^{(+)}(kr) \simeq e^{ikr}/kr$ and the following completeness relation for the Clebsch-Gordan coefficients:

$$\begin{aligned} \sum_{l_1} (-1)^{l_1} [C(l l_p l_1; 000)]^2 &\equiv \sum_{l_1} (-1)^{l_1} \langle l l_p 00 | l_1 0 \rangle \langle l_1 0 | l l_p 00 \rangle \\ &= (-1)^{l+l_p} \sum_{l_1} \langle l l_p 00 | l_1 0 \rangle \langle l_1 0 | l l_p 00 \rangle \\ &= (-1)^{l+l_p} \end{aligned} \quad (5.26)$$

which holds since $C(l_l l_p; 000)$ is different from zero only if $l + l_p + l_1 = \text{even}$. We get

$$\frac{1}{2l+1} \sum_m \text{Im} \chi_{L,L}^{(2)} = (-1)^{l+1} \sum_{p \neq a} \text{Im} \left[e^{2i\delta_l^{(A)}} \frac{e^{2ikR_{pa}}}{(kR_{pa})^2} \left(\sum_{l_p} (2l_p+1) t_{l_p}^p (-1)^{l_p} \right) \right]. \quad (5.27)$$

Using now (4.25) for $\vartheta = \pi$ and (5.19), we see that the expression in large brackets on the RHS is just $-kf_p(\pi)$. We finally obtain

$$\frac{1}{2l+1} \sum_m \text{Im} \chi_{L,L}^{(2)} = (-1)^l \sum_{p \neq a} \text{Im} \left(e^{2i\delta_l^{(A)}} \frac{e^{2ikR_{pa}}}{kR_{pa}^2} f_p(\pi) \right) \quad (5.28)$$

which coincides with the momentum space equation (4.32) (unpolarized beam of x-rays).

Let us discuss the validity of the PWA in this case. In fact, at variance with the momentum space approach (see (4.14) and the following), here the angular momentum l_1 , which the Hankel function belongs to, is not fixed. In (5.25) we sum over all possible values of l_1 satisfying the triangular relation with angular momenta l and l_p (with the only restriction that $l_1 + l + l_p = \text{even}$). Now l is fixed ($l = l_i \pm 1$), but l_p is the angular momentum scattered from the atom P , and we have to judge its range of values.

Consider first high energy: one expects significant scattering contributions from atom P up to $l_p^{\max} = ka$, where a is the atom core radius. The evaluation of the relative correction to the phase of the Hankel function in (5.25) then goes as follows (take the second term in square brackets of (4.17)):

$$\frac{l_1(l_1+1)}{2k^2 R_{pa}^2} \approx \frac{l_p(l_p+1)}{2k^2 R_{pa}^2} < \frac{(l_p^{\max})^2}{2k^2 R_{pa}^2} = \frac{1}{2} \left(\frac{a}{R_{pa}} \right)^2 \ll 1. \quad (5.29)$$

Therefore, in the high-energy region, the smaller $(a/R_{pa})^2$ the more appropriate it is to forget about correcting the phase and the better the PWA works. As discussed in section 4, to hold good the PWA must be applied together with the small-atom approximation.

In the low-energy region, we cannot apply the l_p^{\max} -argument given above; there are only a few (low) values of l_1 that count and we must then require

$$E \gg \hbar^2 l_1(l_1+1)/(4mR_{pa}^2) \quad (5.30)$$

which is an energy bound similar to (4.19).

Therefore, as already seen in section 4, at energies close to the absorption edge, the PWA fails† and one must resort to the exact curved-wave theory (5.20)–(5.25).

† For single scattering, an improved *spherical-wave approximation* [31, 35, 40], obtained by retaining in (5.25) the first correction to the phase and to the modulus of the Hankel function has yielded an excellent agreement with the experimental data down to 20 eV above the K edge of Cu.

5.2. Inelasticities and disorder

The multiple-scattering function $\chi_{LL'}^{(s)}$ must still be corrected for all kinds of inelasticity and disorder. These corrections amount to overall dampings of each term of the perturbative expansion and can therefore improve its convergence.

Inelasticities. All types of inelasticities, electron-electron scattering and finite core-hole lifetime are usually taken care of by the introduction of a damping factor. This can be understood as follows: phenomenologically, the above processes, being absorptions from the elastic scattering channel, are described by adding an imaginary part $-i|V_I|$ to the Hamiltonian H_I . To first approximation, V_I/\hbar is equal in magnitude to the sum of the inverse lifetimes of the core hole and of the active electron. If we suppose that V_I is constant, we get a very simple expression for the new complex electron momentum:

$$k \rightarrow [(2m/\hbar^2)(E + i|V_I|)]^{1/2} \underset{\text{small } V_I}{\approx} k + im|V_I|/\hbar^2 k \quad (5.31)$$

where E is the (real) photoelectron kinetic energy. In the RHS, k is the real part of the photoelectron momentum. The important correction for the multiple-scattering function (5.20)–(5.22) applies to the energy dependence of the g -propagators. All Hankel functions have a small imaginary part in their argument, and this then provides a damping of the term. This is seen quite nicely in the S -propagators of the momentum space approach which yield, in fact, a damping exponential:

$$S_{qp} \rightarrow (e^{ikR_{qp}}/R_{qp})e^{-R_{qp}/\lambda} \quad (5.32)$$

where λ , to be interpreted as the mean free path of the electron, is given by

$$\lambda = \left\{ \text{Im}[(2m/\hbar^2)(E + i|V_I|)]^{1/2} \right\}^{-1} \underset{\text{small } V_I}{\approx} \hbar^2 k/m|V_I|. \quad (5.33)$$

This argument roughly takes into account the effect of inelasticities. In reality, this is not so easy; a complete many-channel treatment of the problem is in fact in order [63]. For simplicity, researchers maintain the mean free path damping argument, multiplying the $\chi^{(s)}$ -function by a correcting (energy-dependent) factor $\eta^{(s)} < 1$. One has also to keep in mind that λ may not be isotropic.

The presence of damping 'penalizes' long closed-loop diagrams such as those involving single scatterings from distant coordination shells (unless shadowing is present), or multiple scatterings with many legs. This is nicely seen in the S -propagators, which become

$$\eta^{(s)} e^{ikR_{\text{tot}}} e^{-R_{\text{tot}}/\lambda} / R_1 R_2 \dots R_s \quad R_{\text{tot}} \equiv R_1 + R_2 + \dots + R_s. \quad (5.34)$$

The peaks in the EXAFS and XANES structures, besides being reduced in amplitude due to the escape of flux, are broadened due to the appearance of complex momenta (to see this in the final formulas, do not make the approximation for V_I small!).

Disorder. As far as disorder is concerned, from quantum mechanics we know that the distance R_{qp} between two generic atoms P and Q cannot be fixed. Besides, in molecules or condensed systems the position of an atom fluctuates because of thermally induced vibrations. More disorder is found in solutions, amorphous systems and glasses.

What happens in practice is that, with the absorption process being faster than any molecular motion, an instantaneous fixed atomic distribution is observed; the experimenter collects several 'snapshots' over a time long compared with the vibration periods, and therefore measures a time average of this distribution.

We shall discuss here the case of single scattering, $s = 2$; for general treatments see [30, 39]. For simplicity we shall discuss the approximate EXAFS formula (4.30).

The time average is profitably replaced by an average of (4.30) over all spatial configurations of the bond distances R_{pa} . We write

$$R_{pa} = R_{pa}^{(0)} + u_{pa} \quad (5.35)$$

where $u_{pa} \equiv u_p - u_a$. Here u_j is the j th atom displacement vector. We then expand R_{pa} by retaining only terms to first order in u_{pa} :

$$R_{pa} \cong R_{pa}^{(0)} + u_{pa} \cdot R_{pa}^{(0)} / R_{pa}^{(0)}. \quad (5.36)$$

The average of (4.30) affects the sine function most of all. We shall evaluate the remaining part of the EXAFS function (including the damping factors $\exp(-R_{pa}/\lambda)$) at the equilibrium positions $R_{pa} = R_{pa}^{(0)}$. We make the further approximation of averaging, using a Gaussian distribution, only over the variable $u \equiv u_{pa} \cdot R_{pa}^{(0)} / R_{pa}^{(0)}$, neglecting the effects of atomic vibrations orthogonal to the bond direction R_{pa} .

Defining the phase $\Delta_p = 2kR_{pa}^{(0)} + 2\delta_1^{(A)} + \Phi_p$, the evaluation of the average of the sine function appearing in the p th-atom term of (4.30) is straightforward:

$$\frac{1}{\sigma_p(2\pi)^{1/2}} \int_{-\infty}^{+\infty} \sin(2ku + \Delta_p) e^{-u^2/2\sigma_p^2} du = e^{-2k^2\sigma_p^2} \sin \Delta_p. \quad (5.37)$$

The variance σ_p^2 is of course temperature dependent and is interpreted [16, 45] as $[\overline{u_{pa} \cdot R_{pa}^{(0)} / R_{pa}^{(0)}}]^2$, i.e. as the mean square relative displacement along the bond direction. The damping exponential $\exp(-2k^2\sigma_p^2)$ is usually referred to as the Debye-Waller factor (this is improper; see [45]).

The single-scattering EXAFS formula (4.30), corrected for inelasticities and disorder, is then finally given by

$$\begin{aligned} \chi_{10,10}^{(2)(K \text{ edge})} = & -3\eta^{(2)} \sum_{p \neq a} \left(\epsilon \cdot \frac{R_{pa}^{(0)}}{R_{pa}^{(0)}} \right)^2 \frac{|f_p(\pi)|}{k(R_{pa}^{(0)})^2} \\ & \times \sin(2kR_{pa}^{(0)} + 2\delta_1^{(A)} + \Phi_p) e^{-2R_{pa}^{(0)}/\lambda} e^{-2k^2\sigma_p^2}. \end{aligned} \quad (5.38)$$

Equation (5.38) is the most commonly used in applications. As thoroughly discussed in many papers (see reviews [43–50]), a great deal of information can be extracted from (5.38) from comparison with experimental data, using the methods of Fourier transform and filtering, about the local atomic arrangement around the absorbing atom. In particular, one can obtain atomic structure quantities such as bond distances (with accuracies as good as ± 0.01 Å), coordination numbers and mean square displacements.

Some attention must be paid to the *origin of the energy scale*. Due to the subtleties of the pre-edge region in the absorption of photons from a complex molecular or condensed system, one cannot usually decide (within a few eV) on the position of the absorption edge. The energy origin is then treated as a free parameter in order to obtain the best fit with the experimental data.

5.3. The full solution

As already pointed out, electron scattering becomes strong at low energies so, as we approach the absorption edge from above, more and more terms of the perturbative expansion are needed to describe the behaviour of the cross section. In general, the EXAFS (high-energy) region, where only single scatterings are relevant (as pointed out at the end of section 4, in the case of shadowing, multiple scatterings are also relevant in the high-energy region), merges into the XANES region where multiple scatterings become important. Then, very close to the edge, because of the non-convergence of the multiple-scattering series, one needs to use the full non-perturbative solution.

Let us consider this point in some more detail. The perturbative expansion (5.22) can be summed. Define the matrices:

$$(\tau)_{L_q L_p}^{qp} = \tau_{L_q L_p}^{qp} \quad (t)_{L_q L_p}^{qp} = t_{l_p}^p \delta_{qp} \delta_{L_q L_p} \quad (g)_{L_q L_p}^{qp} = (1 - \delta_{qp}) g_{L_q L_p}(\mathbf{R}_{qp}). \quad (5.39)$$

Using (5.39) in (5.22) yields immediately the matrix equation

$$\tau = t + tg\tau \quad (5.40)$$

which is easily solved for τ :

$$\tau = (1 - tg)^{-1} t = (t^{-1} - g)^{-1}. \quad (5.41)$$

This is the complete (non-perturbative) solution of our problem expressed in the combined angular-momentum-atomic-site discrete Hilbert space.

The operators $\tau_{L_q L_p}^{qp}$ introduced in this section, via the expansion (5.22), are just the on-shell angular momentum representatives of the τ -operators discussed at the end of section 2. The link is provided by

$$\tau_{L_p L_q}^{pq} = (2m/\hbar^2) k_p \langle j_{l_p} Y_{L_p} | \tau_{pq} | j_{l_q} Y_{L_q} \rangle_q. \quad (5.42)$$

Therefore (5.21), (5.22), (5.40), (5.41) correspond to (2.32), (2.35), (2.28), (2.33), respectively.

At this point a comment on the absolute convergence of the perturbative expansion (5.22)/(2.35) is in order. The expansion (5.22) is written as

$$\tau = (1 - K)^{-1} t = \left(\sum_{n=0}^{\infty} K^n \right) t \quad K \equiv tg. \quad (5.43)$$

Let us diagonalize the matrix $K \equiv tg$: $K_D = B K B^{-1}$, where of course the matrix B also diagonalizes the inverse matrix appearing in (5.43): $B(1 - K)^{-1} B^{-1} = (1 - B K B^{-1})^{-1}$.

The geometric series $\sum_{n=0}^{\infty} K^n$ converges absolutely if the series $\sum_{n=0}^{\infty} (K_D)^n$ does. The diagonal matrix K_D has for diagonal elements just its eigenvalues λ_{σ} . The general criterion for the absolute convergence is then to require that all eigenvalues λ_{σ} be of modulus less than 1:

$$\text{Max} |\lambda_{\sigma}| < 1. \quad (5.44)$$

The eigenvalues λ_σ of K_D are of course the eigenvalues of $K \equiv tg$. They are energy dependent, so the energy axis is divided into regions where (5.44) does or does not hold. These regions are obviously system dependent.

We emphasize that dampings due to inelasticities and disorder when properly introduced, will help the convergence of the perturbative expansion.

The big asset of (5.41) as compared with (2.33) lies in the appearance of discrete matrix multiplication for the on-shell matrix elements rather than continuous (space or momentum) integrations. This allows computation of the full solution (5.41), by properly truncating the dimension of the matrices.

In the literature [65–71] one can find computer codes devised to solve this truncated problem. The calculation is performed on a cluster of atoms for a finite (system-dependent) number of angular momenta. The dimension of the cluster is determined by the maximum round-trip time of flight of the electron compatible with the decay of the photoelectron itself and of the core hole. Usually, the cluster is divided into concentric shells of atoms, with the absorbing atom A at the centre. The multiple-scattering equations (5.41) are solved first within each shell, and then between the shells themselves and the atom A [65, 71]. This procedure has the advantage of replacing the inversion of a very large matrix with a number of smaller inversions, saving on computer times.

With these full-solution calculations, one is able to enter into the energy region of XANES in which $\text{Max}|\lambda_\sigma| \geq 1$, where the perturbative expansion does not converge. They are useful also if $\text{Max}|\lambda_\sigma|$ is less than but close to 1, in which case the convergence of the series is slow. If $\text{Max}|\lambda_\sigma| \ll 1$, then the series converges rapidly, intrashell multiple scattering is not important and one can compute only the first few terms of the expansion instead of the full solution. At high enough energies, the electron-atom scattering becomes weaker and weaker, and one is then allowed to consider (apart from the case of shadowing) only single scatterings (EXAFS region). Eventually, at extremely high energy, one is left only with the atomic absorption (3.15).

Use of the full-solution computer codes in the XANES region yields information that is unobtainable from EXAFS, such as data on bond angles and local geometries. Calculations of XANES can distinguish between different models of local structure, similarly to electron diffraction (LEED) determination of surface structures [58].

Acknowledgments

Supported in part by the University of Trieste and the Istituto Nazionale di Fisica Nucleare.

References

- [1] Kronig R de L 1932 *Z. Phys.* **75** 468
- [2] Petersen H 1932 *Z. Phys.* **76** 768; 1933 *Z. Phys.* **80** 258
- [3] Hartree D R, Kronig R de L and Petersen H 1935 *Physica* **2** 144
- [4] Azaroff L V 1963 *Rev. Mod. Phys.* **35** 1012
- [5] Stumm von Bordwehr R 1989 *Ann. Physique Fr.* **14** 377
- [6] Sayers D E, Lytle F W and Stern E A 1970 *Advances in X-ray Analysis* vol 13, ed B L Henke, J B Newkirk and G R Mallett (New York: Plenum) p 248

- [7] Sayers D E, Stern E A and Lytle F W 1971 *Phys. Rev. Lett.* **27** 1204
- [8] Schaich W L 1973 *Phys. Rev. B* **8** 4028
- [9] Stern E A 1974 *Phys. Rev. B* **10** 3027
- [10] Mazalov L N, Gel'mukhanov F Kh and Chermoshentsev V M 1974 *J. Struct. Chem.* **15** 975
- [11] Lytle F W, Sayers D E and Stern E A 1975 *Phys. Rev. B* **11** 4825
- [12] Stern E A, Sayers D E and Lytle F W 1975 *Phys. Rev. B* **11** 4836
- [13] Ashley C A and Doniach S 1975 *Phys. Rev. B* **11** 1279
- [14] Lee P A and Pendry J B 1975 *Phys. Rev. B* **11** 2795
- [15] Lee P A 1976 *Phys. Rev. B* **13** 5261
- [16] Beni G and Platzman P M 1976 *Phys. Rev. B* **14** 1514
- [17] Teo B-K, Lee P A, Simmons A L, Eisenberger P and Kinkaid B 1977 *J. Am. Chem. Soc.* **99** 3854
- [18] Lee P A and Beni G 1977 *Phys. Rev. B* **15** 2862
- [19] Teo B-K and Lee P A 1979 *J. Am. Chem. Soc.* **101** 2815
- [20] Grosso G and Pastori Parravicini G 1980 *J. Phys. C: Solid State Phys.* **13** L919
- [21] Stern E A, Bunker B A and Heald S M 1980 *Phys. Rev. B* **21** 5521
- [22] Raoux D, Petiau J, Bondot P, Calas G, Fontaine A, Lagarde P, Levitz Y, Loupiau G and Sadoc A 1980 *Revue Phys. Appl.* **15** 1079
- [23] Teo B-K 1981 *J. Am. Chem. Soc.* **103** 3990
- [24] Boland J J, Crane S E and Baldeschwieler J D 1982 *J. Chem. Phys.* **77** 142
- [25] Müller J E and Schaich W L 1983 *Phys. Rev. B* **27** 6489
- [26] Natoli C R 1983 *EXAFS and Near Edge Structure (Springer Series in Chem. Phys. 27)* ed A Bianconi, L Incoccia and S Stipcich (Berlin: Springer) p 43
- [27] Co M S, Hendrickson W A, Hodgson K O and Doniach S 1983 *J. Am. Chem. Soc.* **105** 1144
- [28] Schaich W L 1984 *Phys. Rev. B* **29** 6513
- [29] Gurman S J, Binstead N and Ross I 1984 *J. Phys. C: Solid State Phys.* **17** 143; 1986 *J. Phys. C: Solid State Phys.* **19** 1845
- [30] Boland J J and Baldeschwieler J D 1984 *J. Chem. Phys.* **80** 3005
- [31] Barton J and Shirley D A 1985 *Phys. Rev. B* **32** 1892, 1906
- [32] McKale A G, Knapp G S and Chan S-K 1986 *Phys. Rev. B* **33** 841
- [33] Natoli C R and Benfatto M 1986 *J. Physique Coll.* **47** C8 11
- [34] Natoli C R, Benfatto M and Doniach S 1986 *Phys. Rev. A* **34** 4682
- [35] Rehr J J, Albers R C, Natoli C R and Stern E A 1986 *Phys. Rev. B* **34** 4350
- [36] Strange R W, Blackburn N J, Knowles P F and Hasnain S S 1987 *J. Am. Chem. Soc.* **109** 7157
- [37] Ruiz-Lopez M F, Loos M, Goulon J, Benfatto M and Natoli C R 1988 *Chem. Phys.* **121** 419
- [38] Brouder C, Ruiz-Lopez M F, Pettifer R F, Benfatto M and Natoli C R 1989 *Phys. Rev. B* **39** 1488, 1936
- [39] Benfatto M, Natoli C R and Filipponi A 1989 *Phys. Rev. B* **40** 9626
- [40] Rehr J J and Albers R C 1990 *Phys. Rev. B* **41** 8139
- [41] Filipponi A, Cicco A Di, Benfatto M and Natoli C R 1990 *Europhys. Lett.* **13** 319
- [42] Brouder C and Hikam M 1991 *Phys. Rev. B* **43** 3809
- [43] Stern E A 1978 *Contemp. Phys.* **19** 289
- [44] Brown G S and Doniach S 1980 *Synchrotron Radiation Research* ed H Winick and S Doniach (New York: Plenum) p 353
- [45] Lee P A, Citrin P H, Eisenberger P and Kincaid B M 1981 *Rev. Mod. Phys.* **53** 769
- [46] Stern E A and Heald S M 1983 *Handbook on Synchrotron Radiation* ed E E Koch (Amsterdam: North-Holland) p 955
- [47] Teo B-K 1986 *EXAFS: Basic Principles and Data Analysis* (Berlin: Springer)
- [48] Stern E A 1988 *X-Ray Absorption* ed D C Koningsberger and R Prins (New York: Wiley) p 3
- [49] Durham P J 1988 *X-Ray Absorption* ed D C Koningsberger and R Prins (New York: Wiley) p 53
- [50] Sayers D E and Bunker B A 1988 *X-Ray Absorption* ed D C Koningsberger and R Prins (New York: Wiley) p 211
- [51] Hasnain S S (ed) 1991 *X-Ray Absorption Fine Structure* (New York: Ellis Horwood)
- [52] Schaich W L 1991 *Handbook on Synchrotron Radiation* ed G Brown and D E Moncton (Amsterdam: Elsevier Science) p 505
- [53] Historical papers on multiple scattering include
- [54] Foldy L L 1945 *Phys. Rev.* **67** 107
- [55] Lax M 1951 *Rev. Mod. Phys.* **23** 287
- [56] Ekstein H 1952 *Phys. Rev.* **87** 31

- Watson K M 1953 *Phys. Rev.* **89** 575
- [52] Beeby J L and Edwards S F 1963 *Proc. R. Soc. A* **274** 395
- [53] Johnson K H 1966 *J. Chem. Phys.* **45** 3085; 1973 *Advances in Quantum Chemistry* vol 7, ed P-O Löwdin (New York: Academic) p 143
- [54] Beeby J L 1967 *Proc. R. Soc. A* **302** 113
- [55] Gyorffy B L and Stott M J 1971 *Solid State Commun.* **9** 613; 1973 *Band Structure Spectroscopy of Metals and Alloys* ed D J Fabian and L M Watson (New York: Academic) p 385
- [56] Lloyd P and Smith P V 1972 *Adv. Phys.* **21** 69
- [57] Dill D and Dehmer J L 1974 *J. Chem. Phys.* **61** 692
- [58] Pendry J B 1974 *Low Energy Electron Diffraction* (London: Academic)
- [59] Faulkner J S and Stocks G M 1980 *Phys. Rev. B* **21** 3222
- [60] Kutzler F W, Natoli C R, Misemer D K, Doniach S and Hodgson K O 1980 *J. Chem. Phys.* **73** 3274
- [61] Feder R 1985 *Polarized Electrons in Surface Physics* (Singapore: World Scientific) p 125
- [62] Strange P, Ebert H, Staunton J B and Gyorffy B L 1989 *J. Phys.: Condens. Matter* **1** 2959
- [63] Natoli C R, Benfatto M, Brouder C, Ruiz Lopez M F and Foulis D L 1990 *Phys. Rev. B* **42** 1944
- [64] Müller J E and Wilkins J W 1984 *Phys. Rev. B* **29** 4331
- [65] Durham P J, Pendry J B and Hodges C H 1982 *Comput. Phys. Commun.* **25** 193
- [66] Bianconi A, Dell'Ariccia M, Durham P J and Pendry J B 1982 *Phys. Rev. B* **26** 6502
- [67] Vedrinskii R V, Gegusin I I, Datsyuk V N, Novakovich A A and Kraizman V L 1982 *Phys. Status Solidi B* **111** 433
- [68] Bunker G and Stern E A 1984 *Phys. Rev. Lett.* **52** 1990; 1985 *Phys. Rev. Lett.* **54** 2726
- [69] Vvedensky D D and Pendry J B 1985 *Phys. Rev. Lett.* **54** 2725
- [70] Kitamura M, Muramatsu S and Sugiura C 1986 *Phys. Rev. B* **33** 5294
- [71] Vvedensky D D, Saldin D K and Pendry J B 1986 *Comput. Phys. Commun.* **40** 421
- [72] Heitler W 1954 *The Quantum Theory of Radiation* (London: Oxford)
- Bethe H A and Salpeter E E 1957 *Quantum Mechanics of One- and Two-Electron Systems* (Berlin: Springer)
- [73] Fonda L 1969 *Scattering Theory* ed A O Barut (New York: Gordon and Breach) p 129
- [74] Fano U and Cooper J W 1968 *Rev. Mod. Phys.* **40** 441
- [75] Hedin L and Lundqvist S 1969 *Solid State Physics* vol 23, ed H Ehrenreich, F Seitz and D Turnbull (New York: Academic) p 1
- [76] Rehr J J, Stern E A, Martin M L and Davidson E R 1978 *Phys. Rev. B* **17** 560
- [77] Domke M, Xue C, Puschmann A, Mandel T, Hudson E, Shirley D A and Kaindl G 1990 *Chem. Phys. Lett.* **173** 122
- [78] Bianconi A, Cicco A Di, Pavel N V, Benfatto M, Marcelli A, Natoli C R, Pianetta P and Woicik J 1987 *Phys. Rev. B* **36** 6426
- [79] Tolentino H, Medarde M, Fontaine A, Baudalet F, Dartyge E, Guay F and Tourillon G 1992 *Phys. Rev. B* **45** 8091
- [80] Hitchcock A P 1990 *Phys. Scr.* **T 31** 159
- [81] Piancastelli M N, Ferrett T A, Lindle D W, Medhurst L J, Heimann P A, Liu S H and Shirley D A 1989 *J. Chem. Phys.* **90** 3004
- [82] Fonda L and Ghirardi G C 1970 *Symmetry Principles in Quantum Physics* (New York: Dekker)
- [83] Newton R G 1966 *Scattering Theory of Waves and Particles* (New York: McGraw-Hill)
- [84] Abramowitz M and Stegun I A 1965 *Handbook of Mathematical Functions* (New York: Dover)